HELDA
HELSINGIN YLIOPISTO
HELSINGFORS UNIVERSITET
UNIVERSITY OF HELSINKI

UNIVERSITY OF HELSINKI

https://helda.helsinki.fi

Tropomodulins Control the Balance between Protrusive and Contractile Structures by Stabilizing Actin-Tropomyosin Filaments

Kumari, Reena

2020-03-09

Kumari , R , Jiu , Y , Carman , P J , Tojkander , S , Kogan , K , Varjosalo , M , Gunning , P W , Dominguez , R & Lappalainen , P 2020 , ' Tropomodulins Control the Balance between Protrusive and Contractile Structures by Stabilizing Actin-Tropomyosin Filaments ' , Current Biology , vol. 30 , no. 5 , pp. 767-778.e5 . https://doi.org/10.1016/j.cub.2019.12.049

http://hdl.handle.net/10138/326055
https://doi.org/10.1016/j.cub.2019.12.049

cc_by_nc_nd
acceptedVersion

Downloaded from Helda, University of Helsinki institutional repository.

This is an electronic reprint of the original article.

This reprint may differ from the original in pagination and typographic detail.

Please cite the original version.

Tropomodulins control the balance between protrusive and contractile structures by stabilizing actin-tropomyosin filaments

Reena Kumari[1], Yaming Jiu[1,6,7], Peter J Carman[2,3], Sari Tojkander[4]. Konstantin Kogan[1], Markku Varjosalo[1], Peter W Gunning[5], Roberto Dominguez[2], Pekka Lappalainen[1]*

[1] HiLIFE Institute of Biotechnology, University of Helsinki, Finland

[2] Department of Physiology, Perelman School of Medicine, University of Pennsylvania, Philadelphia, PA, USA

[3] Graduate Group in Biochemistry and Molecular Biophysics, The Perelman School of Medicine, The University of Pennsylvania, Philadelphia, PA, USA

[4] Department of Veterinary Biosciences, Faculty of Veterinary Medicine, University of Helsinki, Finland

[5] School of Medical Sciences, UNSW, Sydney, Australia

[6] CAS Key Laboratory of Molecular Virology and Immunology, Institute Pasteur of Shanghai, Chinese Academy of Sciences, Shanghai, China

[7] University of Chinese Academy of Sciences, Beijing, China

***Corresponding author & lead contact**

Pekka Lappalainen, Institute of Biotechnology, P.O. Box 56, University of Helsinki, 00014, Helsinki, Finland

Email: pekka.lappalainen@helsinki.fi

Phone: +358 50 4155433

SUMMARY

Eukaryotic cells have diverse protrusive and contractile actin filament structures, which compete with one another for a limited pool of actin monomers. Numerous actin-binding proteins regulate the dynamics of actin structures, including tropomodulins (Tmods), which cap the pointed end of actin filaments. In striated muscles, Tmods prevent actin filaments from overgrowing, whereas in non-muscle cells their function has remained elusive. Here, we identify two Tmod isoforms, Tmod1 and Tmod3, as key components of contractile stress fibers in non-muscle cells. Individually, Tmod1 and Tmod3 can compensate for one another, but their simultaneous depletion results in disassembly of actin-tropomyosin filaments, loss of force-generating stress fibers, and severe defects in cell morphology. Knockout-rescue experiments reveal that Tmod's interaction with tropomyosin is essential for its role in the stabilization of actin-tropomyosin filaments in cells. Thus, in contrast to their role in muscle myofibrils, in non-muscle cells Tmods bind actin-tropomyosin filaments to protect them from depolymerizing, not elongating. Furthermore, loss of Tmods shifts the balance from linear actin-tropomyosin filaments to Arp2/3 complex-nucleated branched networks, and this phenotype can be partially rescued by inhibiting the Arp2/3 complex. Collectively, the data reveal that Tmods are essential for the maintenance of contractile actomyosin bundles, and that Tmod-dependent capping of actin-tropomyosin filaments is critical for the regulation of actin homeostasis in non-muscle cells.

Keywords: actin cytoskeleton; mechanosensing; stress fiber; tropomodulin; myosin; formin; Arp2/3 complex; tropomyosin

HIGHLIGHTS

- **Tmods stabilize tropomyosin-decorated actin filaments in non-muscle cells**
- **Actin filament capping by Tmods is essential for contractile stress fibers**
- **Loss of Tmod-stabilized filaments leads to abnormal cell morphology**
- **Tmods control balance between Arp2/3-networks and tropomyosin-actin filaments**

INTRODUCTION

Actin filaments assemble into diverse three-dimensional structures that produce force for various vital processes in cells. These structures include branched actin networks in lamellipodia, which polymerize against the plasma membrane to push the leading edge forward during cell migration. Similar branched actin filament networks also provide force for the generation of plasma membrane invaginations during endocytosis. Actin filaments, together with myosin II filaments, also assemble into contractile structures, where the force is produced by ATP-dependent sliding of bi-polar myosin II filaments along the antiparallel array of actin filaments [1, 2]. In order to generate these and other functionally distinct actin filament arrays, different actin filament nucleation machineries have evolved. These include the Arp2/3 complex, which nucleates new actin filaments from the sides of pre-existing 'mother filaments' to generate branched actin filament networks that are predominant at the leading edge of motile cells and in the sites of endocytosis. The other major class of actin nucleators are the formins, family of proteins that bind to filament barbed ends to assemble linear arrays of actin filaments that are needed in the contractile actomyosin structures [3, 4].

The protein compositions and dynamic properties of distinct actin filament arrays are markedly different. The Arp2/3 complex-nucleated, branched actin networks display rapid turnover, and proteins that drive rapid actin filament turnover are enriched in these structures [5, 6]. On the other hand, formin-nucleated actin filament arrays are decorated by tropomyosins (Tpm), which stabilize actin filaments and recruit myosins to these structures [7, 8]. Importantly, recent studies showed that different actin assembly factors compete with each other for a limited pool of assembly-competent actin monomers in cells [9, 10]. Consequently, depletion of profilin, a small actin monomer-binding protein that delivers actin monomers to formins and Ena/VASP, results in an excessive assembly of Arp2/3 complex-nucleated actin structures at the expense of formin- and Ena/VASP-assembled actin filament arrays [11, 12]. Thus, a fine balance in actin filament nucleation exists between Arp2/3 complex, formins, as well as Ena/VASP actin polymerizing proteins.

Compared to protrusive actin filament arrays, the actin filaments in contractile actomyosin structures, such as muscle myofibrils and the stress fibers of non-muscle cells, undergo slower turnover [13-15]. Both myofibrils and stress fibers are composed of a bipolar array of myosin II and Tpm-decorated actin filaments. While myofibrils contribute exclusively to muscle contraction, stress fibers are involved in diverse processes, including cell migration, adhesion, morphogenesis, and mechanosensing [16]. Actin filaments in myofibrils are stabilized by CapZ and tropomodulins (Tmods), which cap the barbed and pointed ends of sarcomeric actin filaments, respectively [17].

However, the mechanisms regulating the turnover of actin filaments in stress fibers of non-muscle cells are less well understood.

Tmods interact with the pointed end of an actin filament through their two actin-binding sites. In addition, Tmods contain two Tpm-binding sites, and thus they bind tropomyosin-decorated filaments with higher affinity (Kd ~20 nM) compared to bare actin filaments (Kd ~0.1 – 0.2 μM) [18, 19]. Mammals have four Tmod isoforms, Tmod1, expressed in various post-mitotic cells; Tmod2, expressed in neurons; Tmod3, expressed ubiquitously in different tissues; and Tmod4, mainly in skeletal muscles [20]. All Tmod isoforms cap actin filament pointed ends, but Tmod3 can also bind actin monomers [21]. Genetic studies demonstrated that deletion of the two most widely-expressed isoforms, Tmod1 and Tmod3, results in embryonic lethality in mice [22, 23].

The functions of Tmods have been thoroughly studied in striated muscles, where they localize to the pointed ends of sarcomeric actin filaments. Inactivation of Tmods in fully developed striated muscles results in an increase in the length of thin filaments, while the overexpression resulted in shorter filaments, indicating that they function as negative regulators of actin filament elongation [24, 13, 25, 26]. Similar to striated muscles, Tmods control the regular length of actin filaments in the red blood cell membrane skeleton [27]. On the other hand, the functions of Tmods in other non-muscle cells are less well understood, and whether they prevent actin filaments from overgrowth, stabilize actin filaments or control their organization has remained elusive. Tmods have been linked to exocytosis [28], assembly of cytoplasmic F-actin network in oocytes [29], as well as maintenance of the actin filament network at adherens junctions [30]. Tmod3 also contributes to cell migration and lamellipodia formation, with its depletion resulting in faster cell migration and its over-expression in decreased cell motility in endothelial cells [31]. However, whether Tmod3 functions as a negative regulator of cell migration by sequestering actin monomers, capping the pointed ends of lamellipodial actin filaments, or by some other mechanism is unknown. A recent study also revealed that a GFP-fusion of Tmod3 localizes to the stress fibers in a periodic pattern, similarly to the localization of Tmods in muscle myofibrils [32]. It is unknown, however, if endogenous Tmods also localize to stress fibers, and whether they contribute to stress fiber assembly, maintenance and contractility.

Here, we examined the role of Tmods in human osteosarcoma (U2OS) cells. We reveal that Tmod1 and Tmod3 are critical for the maintenance of Tpm-decorated actin filaments in contractile actin stress fibers, and hence simultaneous depletion of both isoforms led to a loss of stress fibers, and drastic defects in cellular force production. We further show that stabilization of Tpm-decorated actin

filaments by Tmods is critical for maintaining the balance between contractile actomyosin structures and Arp2/3 complex-nucleated branched actin filament networks in non-muscle cells.

RESULTS

Tmod1 and Tmod3 are components of contractile actin stress fibers

To identify novel stress fiber components, we performed a proximity-dependent biotin identification (BioID) analysis on human U2OS osteosarcoma cells by using a core stress-fiber component, tropomyosin-3.1 (Tpm3.1), as a bait. With this approach, we identified pointed end -capping protein Tmod3 among the most abundant Tpm3.1-interaction partners (Table S1). Western blot and immunofluorescence microscopy analyses revealed that, in addition to Tmod3, also Tmod1 is expressed in U2OS cells. We also detected a very weak signal with Tmod4 antibody, whereas Tmod2 was undetectable (Fig. S1A). Immunofluorescence microscopy demonstrated that endogenous Tmod1 and Tmod3 localize to stress fibers in U2OS cells (Fig 1A, and S1B). Tmod3 displayed prominent localization to both contractile (ventral stress fibers and transverse arcs) as well as non-contractile (dorsal stress fibers) actin bundles, whereas endogenous Tmod1 was detected only in contractile actin bundles. Moreover, a small fraction of Tmod3 localized to the lamellipodia (Fig. 1A and S1B). Please note that the observed nuclear localization with the Tmod3 antibody is likely an artifact resulting from unspecific antibody-binding, because similar nuclear staining with this antibody was also observed in Tmod3 knockout cells (Fig. 1B).

To examine the functions of Tmod1 and Tmod3 in U2OS cells, we silenced Tmod1 by siRNA (Fig. 1C) and generated Tmod1 and Tmod3 knockout cell-lines by CRISPR/Cas9 (Fig. 1C, S1G, and S2A-D). Depletion of either isoform did not lead to drastic defects in the stress fiber networks of cells cultured on coverslips or on micro-patterned surfaces (Fig. 1B and S1C-F). Interestingly, Western blot analysis revealed elevated Tmod1 protein levels in the Tmod3 knockout cells compared to control cells (Fig. 1C,D), as well as upregulation of Tmod3 in Tmod1 knockdown cells (Fig. 1C,E). Tmod1 and Tmod3 also localized more prominently to stress fibers in the cells where the other isoform was absent (Fig. 1B). Together, these data show that Tmod1 and Tmod3 are integral components of stress fibers, and may have at least partially redundant roles in stress fiber assembly/maintenance in osteosarcoma cells.

Depletion of Tmods results in the disappearance of stress fibers and in consequent defects in force generation

To address the functional roles of Tmods in stress fibers, we simultaneously depleted Tmod1 and Tmod3 from U2OS cells. This was achieved through acute depletion of Tmod1 by siRNA in the background of Tmod3 knockout cells (Tmod3 KO+Tmod1 siRNA). Wild-type cells, as well as the cells where Tmod1 or Tmod3 were individually depleted, contained prominent stress fibers and mature focal adhesions, but the Tmod3 KO+Tmod1 siRNA cells (lacking both Tmod isoforms) displayed almost complete loss of stress fibers and contained only very small focal adhesions (Fig. 2A). Instead, these cells contained a dense, disorganized meshwork of actin filaments. A similar phenotype was observed in cells in which Tmod1 and Tmod3 were simultaneously depleted by siRNAs (Fig. S2E-I). Quantification of the numbers of thick actin filament bundles revealed a small decrease in the amount of thick stress fibers in Tmod1 and Tmod3 knockout cells (Fig. S1D). However, the numbers of thick actin bundles detected by this approach in Tmod3 KO+Tmod1 siRNA cells were severely reduced compared to control cells (Fig. 2B). Additionally, the proportion of small focal adhesions was much higher in Tmod3 KO+Tmod1 siRNA cells compared to control cells, and cells where the Tmod isoforms were depleted individually (Fig. 2C, and S1E).

Because stress fibers are the major generators of contractile forces in many non-muscle cells [33], we examined the effects of Tmod-depletion on cellular force generation. Tmod3 KO+Tmod1 siRNA cells displayed a significant reduction in traction-force generation compared to wild-type U2OS cells (Fig. 2F,G). Together, these results show that Tmods are critical for maintenance of contractile stress fibers in U2OS cells. Consequently, their depletion results in severe defects in cell morphogenesis, force production, and the maturation of focal adhesions.

Tmods stabilize tropomyosin-decorated actin filaments in non-muscle cells

In mammals, over 40 different tropomyosin isoforms can be generated from four *tropomyosin* genes through alternative splicing. Actin filaments in stress fibers are largely decorated by tropomyosins, which stabilize and functionalize these filaments [7]. Tmods display higher affinity to tropomyosin-decorated actin filament pointed-ends compared to bare actin filaments [18, 19]. Therefore, we compared the localization of tropomyosins in wild-type vs. Tmod3 KO+Tmod1 siRNA cells. Immunofluorescence microscopy using LC24 antibody, which detects tropomyosin isoforms Tpm2.1 and Tpm4.2, revealed that these tropomyosins faithfully localize to stress fibers in wild-type cells, but display more diffuse localization in cells lacking Tmods (Fig. 3A). Because earlier studies reported that many tropomyosin isoforms are unstable and degraded in the absence of actin filament templates [34, 35], we analyzed the protein levels of Tpm1.6/1.7/2.1 with TM311, and Tpm2.1/4.2 and Tpm3.1/3.2 with LC24 and ϒ/9d antibodies, respectively. Western blot analysis revealed that

depletion of Tmod3 alone resulted in only small decreases in Tpm1.6/1.7/4.2 protein levels, whereas the levels of Tpm2.1 and Tmp3.1/3.2 were not significantly affected. When Tmod1 was depleted, the levels of Tpm1.6/1.7/2.1 were unaltered, whereas the levels of Tpm2.1/4.2/3.1/3.2 were elevated compared to control cells. However, when both Tmod3 and Tmod1 were depleted, cells showed drastically lower levels of all the tropomyosin isoforms (Fig. 3B,C).

Quantitative real-time polymerase chain-reaction (qRT-PCR) analysis revealed that the mRNA levels of Tpm1.7, Tpm3.1, and Tpm4.2 were not diminished by simultaneous depletion of Tmod1 and Tmod3, demonstrating that the decreases in the protein levels of these isoforms do not result from lower transcript levels. In contrast, the mRNA levels of Tpm1.6, which is generated through alternative splicing from the same gene as Tpm1.7, were drastically reduced in the Tmod3 KO+Tmod1 siRNA cells (Fig. S3B). However, the Tpm1.6 mRNA levels were similarly diminished in Tmod1 siRNA cells and Tmod3 KO cells (Fig. S3C), which do not display a strong stress fiber phenotype (Fig. 1B, and S3A). Thus, although the depletion of Tmod1 and Tmod3 (either individually or together) affects the alternative splicing of *TPM1* gene, the resulting decrease in the Tpm1.6 mRNA level does not affect the organization of stress fibers.

In addition to the loss of stress fibers, the Tmod–depleted cells typically contained more pronounced lamellipodia-like protrusions, as detected by an antibody against the Arp2/3 complex, compared to the wild-type U2OS cells (Fig. 2D,E). To further test whether the loss of Tpm-decorated actin filaments, and an increase of lamellipodial width result from Tmod depletion, we performed rescue experiments using GFP-tagged Tmod3 (GFP-Tmod3). The cells were stained with phalloidin to visualize F-actin, with LC24 antibody to visualize Tpm2.1/Tpm4.2, and with cortactin and Arp2/3 antibodies to visualize Arp2/3-rich lamellipodia-like protrusions. Expression of GFP-Tmod3 in the Tmod3 KO+Tmod1 siRNA cells led to a re-appearance of stress fibers that also contained tropomyosins (Fig. 4A). Moreover, the total tropomyosin intensities were higher in rescue cells compared to the Tmod-depleted cells that did not express GFP-Tmod3 (Fig. 4B). Finally, the increased lamellipodial width in Tmod-depleted cells was rescued by expressing GFP-Tmod3 (Fig. 4A,C).

We also examined the roles of Tmod1 and Tmod3 in human dermal fibroblasts (HDFs). Simultaneous depletion of Tmod1 and Tmod3 by siRNA in these cells resulted in a depletion of tropomyosin isoforms and a concomitant reduction of stress fibers, similar to what was observed in U2OS cells (Fig. S3D-F). However, we did not observe robust lamellipodia formation in Tmod1/Tmod3 siRNA

cells compared to wild-type HDF cells. This is most likely due to lack of lamellipodia in HDF cells, at least when plated on fibronectin. Together, these results provide evidence that Tmods are critical for maintaining the stability of tropomyosin-decorated actin filaments in non-muscle cells. In the absence of Tmods, most tropomyosins do not associate with actin filaments and are destined for degradation.

The interaction with tropomyosin is essential for Tmod's function *in vitro* and in cells

In addition to an actin-binding site (ABS1), the N-terminal region of Tmods harbors two tropomyosin-binding sites (TMBS1 and TMBS2) [19]. The TMBSs are important for capping Tpm-decorated actin filaments with high-affinity *in vitro* [20, 18]. However, the functional importance of the two TMBSs and Tmod-Tpm interactions in the context of actin dynamics has not been addressed. We mutated the TMBS1 and TMBS2 domains of Tmod3. The mutant was generated by replacing highly-conserved leucine residues with aspartic acid at four locations in TMBS1 (L29D, L32D, L36D, L39D) and TMBS2 (L131D, L134D, L138D, L143D), which should disrupt interactions with the Tpm coiled-coil (Fig. 5A). Using the pyrene-actin fluorescence assay, we determined the maximum elongation rate of actin in the presence of wild-type and mutant Tmod3, both with and without Tpm. Representative experiments illustrate the fluorescence increase upon incorporation of actin monomers into Tmod3-capped actin filaments at various concentrations of Tmod3 (Fig. S4A,C). Saturating CapZ (25 nM) was added to block monomer incorporation into the barbed end of the filaments [18]. Instantaneous slopes were calculated to determine the time intervals corresponding to the maximum elongation rate at each Tmod3 concentration (Fig. S4B,D), and normalized to the control maximum elongation rate in the absence of Tmod. In the absence of Tpm, wild-type and mutant Tmod3 showed equal capping activities (Fig. 5B), whereas in the presence of Tpm the mutant had significantly reduced capping activity (Fig. 5C, S4E,F). These results suggest that the TMBSs of Tmod3 are critical for the binding of Tpm and efficient filament pointed end capping *in vitro*.

Given the reduced capping activity of Tmod3-TMBS mutant in the *in vitro* assays, we performed rescue experiments by expressing wild-type GFP-Tmod3 and the GFP-Tmod3 TMBS mutant in Tmod3 KO+Tmod1siRNA cells. Wild-type GFP-Tmod3 was either detected in stress fibers or displayed rather diffuse localization, depending on the expression level. Importantly, wild-type GFP-Tmod3 was able to rescue the disrupted stress fibers in Tmod-depleted cells, but the Tmod3 TMBS mutant displayed mainly diffuse cytoplasmic or nuclear localization, and failed to rescue the stress fibers phenotype (Fig. 5D,E and S5A,B). Moreover, wild-type Tmod3 rescued the focal adhesion size distribution defect close to the control cell level, but the Tmod3 TMBS mutant expression could not

rescue this phenotype (Fig. S5C). Finally, expression of wild-type GFP-Tmod3 partially rescued the loss of tropomyosins in Tmod3 KO+Tmod1siRNA cells, whereas the Tmod3 TMBS mutant was much less efficient in rescuing the diminished levels of tropomyosins in these cells (Fig. 5F, S5D). Together, these data uncover a functional role of tropomyosin-binding sites (TMBS) of Tmod in its ability to promote efficient pointed end capping of tropomyosin-decorated actin filaments *in vitro*, and in stabilization of tropomyosin-decorated actin filament structures in cells.

Tmods maintain the balance between tropomyosin-actin filaments and Arp2/3 complex-assembled actin filament structures

In unicellular yeasts, tropomyosin-decorated actin filaments are nucleated and polymerized by formins [36, 37], whereas protrusive branched actin networks do not contain detectable levels of tropomyosins, and are mainly nucleated by the Arp2/3 complex [6]. Therefore, we examined the possible connections between Tmod-stabilized tropomyosin-actin filaments and the Arp2/3 complex. We first inhibited Arp2/3 complex by incubating wild-type U2OS cells in the presence of 100 μM CK666, a well-established Arp2/3 complex inhibitor [38]. The tropomyosin levels were not drastically altered, and stress fibers were still present in CK666-treated cells. However, instead of a combination of ventral stress fibers, transverse arcs, and dorsal stress fibers, the Arp2/3 complex-inhibited cells contained predominantly ventral stress fibers that were anchored to large focal adhesions at both the ends (Fig. S6B-F). The efficiency of CK666 treatment was confirmed with an antibody against P34, which demonstrated that Arp2/3 complex localized to lamellipodial edges in wild-type U2OS cells, but was largely absent from lamellipodia of CK666 treated cells (Fig. S6B).

Importantly, treatment of Tmod1/3-depleted cells with the Arp2/3 complex-inhibitor led to a partial rescue of the phenotype. This is because CK666-treated Tmod3 KO+Tmod1 siRNA cells harbored more stress fibers compared to the untreated cells (Fig. 6A). They also displayed larger focal adhesions, and were less circular (Fig. 6B,C). Moreover, treatment of Tmod3 KO+Tmod1 siRNA cells with CK666 led to elevated tropomyosin protein levels, and we could also detect some tropomyosin localization to stress fibers in these cells (Fig. 6E, S6A). Similar rescue of the stress fiber phenotype and tropomyosin levels was also observed when the ARPC2 subunit of the Arp2/3 complex was depleted by siRNA in the Tmod3 KO+Tmod1 siRNA cells (Fig. 6A,D,E).

Taken together, these data provide evidence that Tmods stabilize tropomyosin-actin filaments in non-muscle cells. Depletion of Tmods leads to an unbalance between tropomyosin-actin filaments and

Arp2/3-nucleated branched actin filament structures, and this can be partially rescued by inhibition of the Arp2/3 complex.

DISCUSSION

The function of Tmods has been best characterized in the context of muscle myofibrils, where they prevent actin filaments from overgrowth. Here, we show that in non-muscle cells (U2OS osteosarcoma cell-line and human dermal fibroblasts), Tmods do not prevent actin filaments from excessive growth, but are instead critical for stabilizing tropomyosin-decorated actin filaments. In the absence of Tmods, the tropomyosin-decorated actin filaments disassemble. This also leads to degradation of tropomyosins, because most tropomyosins are unstable in the absence of an actin filament template [35]. At least in budding yeast, tropomyosin-decorated actin filaments are nucleated and elongated by formins [36, 37]. Thus, we propose that depletion of Tmods results in a shift in the balance between formin- and Arp2/3 complex-nucleated actin filament networks, and leads to a consequent loss of stress fibers and in an excess of Arp2/3 complex-nucleated, branched actin filament networks (Fig. 7). Previous studies demonstrated that the Arp2/3 complex-nucleated and formin- & Ena/VASP-polymerized actin filament structures compete with each other for a limited pool of assembly-competent actin monomers in cells. Small actin monomer-binding protein, profilin, controls the homeostasis between these networks by preferentially delivering actin monomers to Ena/VASP and formins [12, 11]. Our results show that, not only regulation of actin filament assembly, but also regulation of actin filament disassembly by Tmods is critical for maintenance of the homeostasis between these actin filament networks in cells. Our data also suggest that tropomyosin-decorated actin filaments have a higher need for filament pointed end stabilization compared to the branched Arp2/3 complex-nucleated networks. This may be because within the branched actin filament networks, majority of filament pointed ends are capped by the Arp2/3 complex, at least until the filaments become severed by ADF/cofilins [39]. This may provide an explanation for the importance of Tmods in stabilizing tropomyosin-decorated, linear actin filaments in non-muscle cells. Moreover, the lamellipodial actin filament networks are more dynamic compared to stress fibers [15, 5]. Thus, actin filament assembly is probably slower in stress fibers compared to Arp2/3-nucleated networks, and thus also filament disassembly must be slower in stress fibers to maintain the balance between these actin filament arrays.

Our data suggest that Tmods have different effects on actin dynamics in myofibrils of muscle vs. stress fibers of non-muscle cells. Previous studies demonstrated that Tmods are negative regulators

of thin filament length in muscle cells [13, 25, 26], while our work demonstrates that loss of Tmods leads to disassembly of functionally similar actin filaments in contractile stress fibers. In this context, it is important to note that actin filament assembly appears to display differences in muscle vs. non-muscle cells. This is because actin filaments in muscle sarcomeres can elongate through actin filament assembly at both filament barbed and pointed ends [13], whereas actin filament elongation in non-muscle cells occurs predominantly through filament polymerization at barbed ends. We speculate that the sizes of actin monomer pools may differ between muscle and non-muscle cells. A large pool of assembly-competent actin monomers in muscle cells would allow filament elongation at both barbed and pointed ends, and thus depletion of Tmods results in overgrowth of tropomyosin-decorated actin filaments. On the other hand, non-muscle cells may have a limited pool of assembly-competent actin monomers [11], and thus depletion of Tmods does not accelerate elongation of tropomyosin-decorated actin filaments at their pointed ends, but instead leads to their depolymerization. Alternatively, the differences in the roles of Tmods in muscle vs. non-muscle cells may result from different actin and tropomyosin isoforms expressed in these cells. In a wider context, these data imply that the same biochemical activity of an actin-binding protein can have opposite effects in cells depending on the cell-type.

Our work provides mechanistic insights into the function of Tmods in non-muscle cells. Previous studies linked Tmods to cell migration, insulin-stimulated exocytosis, and formation of adherens junctions in epithelial cells [31, 30, 28]. Moreover, actin filament and tropomyosin (Tpm4.2) organizations are abnormal in *Tmod3(-/-)* embryo megakaryocytes during platelet biogenesis [23], and mouse lenses lacking Tmod1 were reported to have diminished levels of γ (Tpm3)-tropomyosin [40, 41]. However, the precise mechanism by which Tmods contribute to these processes has remained elusive. We propose that Tmods control these processes though stabilization of tropomyosin-decorated actin filaments, and by maintaining the homeostasis between the Arp2/3 complex- and formin-nucleated actin filament networks. For example, Tmod3 was shown to be a negative regulator of actin filament assembly at lamellipodia [31]. This can be explained by our work demonstrating that inhibition of Tmods increases the amounts of Arp2/3 complex-nucleated actin filaments in cells. Because in addition to stress fibers, Tmod3 also localizes to lamellipodia, it possible that Tmod3 additionally stabilizes specific tropomyosin-decorated actin filaments within the lamellipodium. Indeed, previous studies reported that, in addition to the Arp2/3 complex-nucleated actin filament networks, lamellipodia also contain actin filaments decorated by tropomyosins [42]. Also adherens junctions are composed of both Arp2/3 complex-nucleated actin filament structures as well as tropomyosin-containing contractile actin filament arrays [43, 44]. Thus, depletion of Tmod3

may shift the balance between different actin filament structures, like shown here for U2OS cells, and result in consequent problems in epithelial morphogenesis. Finally, insulin-stimulated exocytosis was shown to involve at least one tropomyosin isoform (Tpm3.1) [28, 45]. Thus, it is possible that also in this process Tmod3 stabilizes Tpm3.1-decorated actin filaments that are necessary for exocytosis.

Collectively, our work reveals that Tmods specifically cap tropomyosin-decorated actin filaments in cells. Depending on the cell-type, and probably on the size of assembly-competent actin monomer pool, Tmods either stabilize tropomyosin-decorated actin filaments or prevent them from excessive polymerization. Through their ability to stabilize tropomyosin-decorated actin filaments, Tmods are critical for maintaining the homeostasis between protrusive (Arp2/3 complex-nucleated) and contractile (formin-nucleated) actin filament networks at least in non-muscle cells. An important remaining question concerns the need of several different Tmod isoforms in mammals. Our work demonstrates that Tmod1 and Tmod3 have redundant functions in stabilizing the tropomyosin-decorated actin filament structures in osteosarcoma cells. However, Tmod1 and Tmod3 display minor differences in their subcellular localizations, and their individual depletions resulted in slightly different phenotypes e.g. concerning the protein levels of tropomyosin isoforms. It is possible that different Tmod isoforms exhibit some specificity towards certain tropomyosin isoforms, and may thus stabilize partially non-overlapping populations of tropomyosin-decorated actin filaments in cells. Moreover, Tmod isoforms display biochemical differences. This is because, in addition to actin filament pointed end capping, Tmod3 can bind and sequester actin monomers at least *in vitro* [21]. The possible *in vivo* importance of this activity of Tmod3 should be examined in the future. Finally, Tmods have been associated with various diseases. Elevated levels of Tmod1 and Tmod3 were linked to progression of oral and liver cancers, respectively [46, 47]. Tmod3 was also associated to chemoresistance of non-small cell lung cancer [48]. In the future, it will be important to uncover the precise mechanisms by which Tmods contribute to these human disorders.

ACKNOWLEDGMENTS

The authors thank Velia Fowler for discussions. This study was supported by grants from Sigrid Juselius Foundation, Jane and Aator Erkko Foundation, and Cancer Society Finland (to PL). YJ was supported by "100 talents program" from the Chinese Academy of Sciences; Shanghai Talents Development Funding, National Natural Science Foundation of China (31970660) and Natural Science Foundation of Shanghai (19ZR1463000). Reena Kumari was supported by a PhD-student fellowship from Doctoral School in Health Sciences. PWG received grants from the Australian

National Health and Medical Research Council. PC and RD were supported by NIH grants T32 AR053461 and R01-GM073791, respectively.

AUTHOR CONTRIBUTIONS

R.K., Y.J., R.D. and P.L. designed the study. Y.J. performed BioID screening and generated Tmod3 knock-out cell line. P.J.C. carried out protein purification, pointed-end capping assays and analysed the data. S.T. provided traction force dishes and performed data analysis. K.K. and R.K. analysed the sequencing data. M.V. performed the BioID analysis. P.W.G provided the tropomyosin antibodies. R.K. performed all the remaining experiments, data analysis, and data interpretation. R.K. and P.L. wrote the manuscript, with input from all other authors.

DECLARATION OF INTERESTS

The authors except for PWG declare no competing interests. PWG is a Director and shareholder of TroBio Therapeutics, a company which is developing anti-tropomyosin drugs for the treatment of cancer.

REFERENCES

1. Blanchoin, L., Boujemaa-Paterski, R., Sykes, C., & Plastino, J. (2014). Actin Dynamics, Architecture, and Mechanics in Cell Motility. *Physiological Reviews*, *94*(1), 235–263. https://doi.org/10.1152/physrev.00018.2013

2. Lehtimäki, J. I., Fenix, A. M., Kotila, T. M., Balistreri, G., Paavolainen, L., Varjosalo, M., Burnette, T. D., & Lappalainen, P. (2017). UNC-45a promotes myosin folding and stress fiber assembly. *Journal of Cell Biology*, *216*(12), 4053–4072. https://doi.org/10.1083/jcb.201703107

3. Campellone, K. G., & Welch, M. D. (2010). A nucleator arms race: Cellular control of actin assembly. *Nature Reviews Molecular Cell Biology*, *11*(4), 237–251. https://doi.org/10.1038/nrm2867

4. Skau, C. T., & Waterman, C. M. (2015). Specification of Architecture and Function of Actin Structures by Actin Nucleation Factors. *Annual Review of Biophysics*, *44*(1), 285–310. https://doi.org/10.1146/annurev-biophys-060414-034308

5. Lai, F. P. L., Szczodrak, M., Block, J., Faix, J., Breitsprecher, D., Mannherz, H. G., Stradal, E. B. T., Dunn, A. G., Small, V. J., & Rottner, K. (2008). Arp2/3 complex interactions and actin network turnover in lamellipodia. *EMBO Journal*, *27*(7), 982–992. https://doi.org/10.1038/emboj.2008.34

6. Michelot, A., & Drubin, D. G. (2011). Building distinct actin filament networks in a common cytoplasm. *Current Biology*, *21*(14), R560–R569. https://doi.org/10.1016/j.cub.2011.06.019

7. Gunning, P. W., Hardeman, E. C., Lappalainen, P., & Mulvihill, D. P. (2015). Tropomyosin - master regulator of actin filament function in the cytoskeleton. *Journal of Cell Science*, *128*(16), 2965–2974. https://doi.org/10.1242/jcs.172502

8. Gateva, G., Kremneva, E., Reindl, T., Kotila, T., Kogan, K., Gressin, L., Gunning, P. W., Manstien, D. J., Michelot, A., & Lappalainen, P. (2017). Tropomyosin Isoforms Specify Functionally Distinct Actin Filament Populations In Vitro. *Current Biology*, *27*(5), 705–713. https://doi.org/10.1016/j.cub.2017.01.018

9. Burke, T. A., Christensen, J. R., Barone, E., Suarez, C., Sirotkin, V., & Kovar, D. R. (2014). Homeostatic actin cytoskeleton networks are regulated by assembly factor competition for monomers. *Current Biology*, *24*(5), 579–585. https://doi.org/10.1016/j.cub.2014.01.072

10. Suarez, C., & Kovar, D. R. (2016). Internetwork competition for monomers governs actin cytoskeleton organization. *Nature Reviews. Molecular Cell Biology*, 17(12), 799–810. https://doi.org/10.1038/nrm.2016.106

11. Rotty, J. D., Wu, C., Haynes, E. M., Suarez, C., Winkelman, J. D., Johnson, H. E., Haugh, J. M., Kovar, D. R., & Bear, J. E. (2015). Article Profilin-1 Serves as a Gatekeeper for Actin Assembly by Arp2 / 3-Dependent and -Independent Pathways. *Developmental Cell*, *32*(1), 54–67. https://doi.org/10.1016/j.devcel.2014.10.026

12. Suarez, C., Carroll, R. T., Burke, T. A., Christensen, J. R., Bestul, A. J., Sees, J. A., James, M. L., Sirotkin, V., & Kovar, D. R. (2015). Profilin regulates F-Actin network homeostasis by favoring formin over Arp2/3 complex. *Developmental Cell*, *32*(1), 43–53. https://doi.org/10.1016/j.devcel.2014.10.027

13. Littlefield, R., Almenar-Queralt, A., & Fowler, V. M. (2001). Actin dynamics at pointed ends regulates thin filament length in striated muscle. *Nature Cell Biology*, *3*(6), 544–551. https://doi.org/10.1038/35078517

14. Skwarek-Maruszewska, A., Hotulainen, P., Mattila, P. K., & Lappalainen, P. (2009). Contractility-dependent actin dynamics in cardiomyocyte sarcomeres. *Journal of Cell Science*, *122*(12), 2119–2126. https://doi.org/10.1242/jcs.046805

15. Hotulainen, P., & Lappalainen, P. (2006). Stress fibers are generated by two distinct actin assembly mechanisms in motile cells. *Journal of Cell Biology*, *173*(3), 383–394. https://doi.org/10.1083/jcb.200511093

16. Tojkander, S., Gateva, G., & Lappalainen, P. (2012). Actin stress fibers - assembly, dynamics and biological roles. *Journal of Cell Science*, *125*(8), 1855–1864. https://doi.org/10.1242/jcs.098087

17. Cooper, J. A., & Schafer, D. A. (2000). Control of actin assembly and disassembly at filament ends. *Current Opinion in Cell Biology*, *12*(1), 97–103. https://doi.org/10.1016/S0955-0674(99)00062-9

18. Rao, J. N., Madasu, Y., & Dominguez, R. (2014). Mechanism of actin filament pointed-end capping by tropomodulin. *Science*, *345*(6195), 463–467. https://doi.org/10.1126/science.1256159

19. Fowler, V. M., & Dominguez, R. (2017). Tropomodulins and Leiomodins: Actin Pointed End Caps and Nucleators in Muscles. *Biophysical Journal*, *112*(9), 1742–1760. https://doi.org/10.1016/j.bpj.2017.03.034

20. Parreno, J., & Fowler, V. M. (2018). Multifunctional roles of tropomodulin-3 in regulating actin dynamics. *Biophysical Reviews*, *10*(6), 1605–1615. https://doi.org/10.1007/s12551-018-0481-9

21. Fischer, R. S., Yarmola, E. G., Weber, K. L., Speicher, K. D., Speicher, D. W., Bubb, M. R., & Fowler, V. M. (2006). Tropomodulin 3 binds to actin monomers. *Journal of Biological Chemistry*, *281*(47), 36454–36465. https://doi.org/10.1074/jbc.M606315200

22. Fritz-Six, K. L., Cox, P. R., Fischer, R. S., Xu, B., Gregorio, C. C., Zoghbi, H. Y., & Fowler, V. M. (2003). Aberrant myofibril assembly in tropomodulin1 null mice leads to aborted heart development and embryonic lethality. *Journal of Cell Biology*, *163*(5), 1033–1044. https://doi.org/10.1083/jcb.200308164

23. Sui, Z., Nowak, R. B., Sanada, C., Halene, S., Krause, D. S., & Fowler, V. M. (2015). Regulation of actin polymerization by tropomodulin-3 controls megakaryocyte actin organization and platelet biogenesis. *Blood*, *126*(4), 520–530. https://doi.org/10.1182/blood-2014-09-601484

24. Gregorio, C. C., Weber, A., Bondad, M., Pennise, C. R., & Fowler, V. M. (1995). Requirement of pointed-end capping by tropomodulin to maintain actin filament length in embryonic chick cardiac myocytes. *Nature*, 377(6544), 83–86. https://doi.org/10.1038/377083a0

25. Gokhin, D. S., Tierney, M. T., Sui, Z., Sacco, A., & Fowler, V. M. (2014). Calpain-mediated proteolysis of tropomodulin isoforms leads to thin filament elongation in dystrophic skeletal muscle. *Molecular Biology of the Cell*, *25*(6), 852–865. https://doi.org/10.1091/mbc.e13-10-0608

26. Gokhin, David S., Ochala, J., Domenighetti, A. A., & Fowler, V. M. (2016). Tropomodulin 1 directly controls thin filament length in both wild-type and tropomodulin 4-deficient skeletal muscle. *Journal of Cell Science*, *129*(1), e1.2-e1.2. https://doi.org/10.1242/jcs.184986

27. Moyer, J. D., Nowak, R. B., Kim, N. E., Larkin, S. K., Peters, L. L., Hartwig, J., Kuypers, A. F., & Fowler, V. M. (2010). Tropomodulin 1-null mice have a mild spherocytic elliptocytosis with appearance of tropomodulin 3 in red blood cells and disruption of the membrane skeleton. *Blood*, *116*(14), 2590–2599. https://doi.org/10.1182/blood-2010-02-268458

28. Lim, C. Y., Bi, X., Wu, D., Kim, J. B., Gunning, P. W., Hong, W., & Han, W. (2015). Tropomodulin3 is a novel Akt2 effector regulating insulin-stimulated GLUT4 exocytosis through cortical actin remodeling. *Nature Communications*, *6*, 1–15. https://doi.org/10.1038/ncomms6951

29. Jo, Y. J., Jang, W. I., Kim, N. H., & Namgoong, S. (2016). Tropomodulin-3 is essential in asymmetric division during mouse oocyte maturation. *Scientific Reports*, *6*, 1–14. https://doi.org/10.1038/srep29204

30. Cox-Paulson, E. A., Walck-Shannon, E., Lynch, A. M., Yamashiro, S., Zaidel-Bar, R., Eno, C. C., Ono, S., & Hardin, J. (2012). Tropomodulin protects α-catenin-dependent junctional-actin networks under stress during epithelial morphogenesis. *Current Biology*, *22*(16), 1500–1505. https://doi.org/10.1016/j.cub.2012.06.025

31. Fischer, R. S., Fritz-Six, K. L., & Fowler, V. M. (2003). Pointed-end capping by tropomodulin3 negatively regulates endothelial cell motility. *Journal of Cell Biology*, *161*(2), 371–380. https://doi.org/10.1083/jcb.200209057

32. Hu, S., Dasbiswas, K., Guo, Z., Tee, Y. H., Thiagarajan, V., Hersen, P., Chew, L. T., Safran, A. S., Zaidel-Bar, R., & Bershadsky, A. D. (2017). Long-range self-organization of cytoskeletal myosin II filament stacks. *Nature Cell Biology*, *19*(2), 133–141. https://doi.org/10.1038/ncb3466

33. Soiné, J. R. D., Brand, C. A., Stricker, J., Oakes, P. W., Gardel, M. L., & Schwarz, U. S. (2015). Model-based Traction Force Microscopy Reveals Differential Tension in Cellular Actin Bundles. *PLOS Computational Biology*, *11*(3), e1004076. https://doi.org/10.1371/journal.pcbi.1004076

34. Jiu, Y., Peränen, J., Schaible, N., Cheng, F., Eriksson, J. E. Krishnan, R. & Lappalainen, P. (2017). Vimentin intermediate filaments control actin stress fiber assembly through GEF-H1 and RhoA. *Journal of Cell Science*, 130, 892–902. https://doi.org/10.1242/jcs.196881

35. Meiring, J. C. M., Bryce, N. S., Wang, Y., Stear, J., Hardeman, E. C., Gunning, P. W. (2018). Co-polymers of Actin and Tropomyosin Account for a Major Fraction of the Human Actin Cytoskeleton. *Current Biology*, *28*(14), 2331-2337.e5. https://doi.org/10.1016/j.cub.2018.05.053

36. Evangelista, M., Pruyne, D., Amberg, D. C., Boone, C., & Bretscher, A. (2002). Formins direct Arp2/3- independent actin filament assembly to polarize cell growth in yeast. *Nature Cell Biology*, *4*, *32-41*. https://doi.org/10.1038/ncb718

37. Alioto, S. L., Garabedian, M. V, Bellavance, D. R., & Goode, B. L. (2016). Tropomyosin and Profilin Cooperate to Promote Formin-Mediated Actin Nucleation and Drive Yeast Actin Cable Assembly. *Current Biology*, *26*(23), 3230–3237. https://doi.org/10.1016/j.cub.2016.09.053

38. Nolen, B. J., Tomasevic, N., Russell, A., Pierce, D. W., Jia, Z., Mccormick, C. D., Hartman, J., Sakowicz, R., & Pollard, T. D. (2009). Characterization of two classes of small molecule inhibitors of Arp2/3 complex. *Nature*, *460*(7258), 1031–1034. https://doi.org/10.1038/nature08231

39. Svitkina, T. M., & Borisy, G. G. (1999). Arp2/3 Complex and Actin Depolymerizing Factor/Cofilin in Dendritic Organization and Treadmilling of Actin Filament Array in Lamellipodia. *The Journal of Cell Biology*, *145*(5), 1009 – 1026. https://doi.org/10.1083/jcb.145.5.1009

40. Nowak, R. B., Fischer, R. S., Zoltoski, R. K., Kuszak, J. R., & Fowler, V. M. (2009). Tropomodulin1 is required for membrane skeleton organization and hexagonal geometry of fiber cells in the mouse lens. *Journal of Cell Biology*, *186*(6), 915–928.

https://doi.org/10.1083/jcb.200905065

41. Gokhin, D. S., Nowak, R. B., Kim, N. E., Arnett, E. E., Chen, A. C., Sah, R. L., Clark, I. J., Fowler, V. M. (2012). Tmod1 and CP49 Synergize to Control the Fiber Cell Geometry, Transparency, and Mechanical Stiffness of the Mouse Lens. *PLoS ONE*, *7*(11). https://doi.org/10.1371/journal.pone.0048734

42. Brayford, S., Bryce, N. S., Schevzov, G., Haynes, E. M., Bear, J. E., Hardeman, E. C., & Gunning, P. W. (2016). Tropomyosin Promotes Lamellipodial Persistence by Collaborating with Arp2 / 3 at the Leading Edge. *Current Biology*, *26*(10), 1312–1318. https://doi.org/10.1016/j.cub.2016.03.028

43. Charras, G., & Yap, A. S. (2018). Review Tensile Forces and Mechanotransduction at Cell – Cell Junctions. *Current Biology*, *28*(8), R445–R457. https://doi.org/10.1016/j.cub.2018.02.003

44. Caldwell, B. J., Lucas, C., Kee, A. J., Gaus, K., Gunning, P. W., Hardeman, E. C., Yap, S. A., & Gomez, G. A. (2014). Tropomyosin isoforms support actomyosin biogenesis to generate contractile tension at the epithelial zonula adherens. *Cytoskeleton*, *71*(12), 663–676. https://doi.org/10.1002/cm.21202

45. Kee, A. J., Chagan, J., Chan, J. Y., Bryce, N. S., Lucas, C. A., Zeng, J., Hook, J., Treutlein, H., Laybutt, D. R., Stehn, J. R., Gunning, P. W., & Hardeman, E. C. (2018). On-target action of anti-tropomyosin drugs regulates glucose metabolism. *Scientific Reports*, 8: 4604. doi: 10.1038/s41598-018-22946-x.

46. Suzuki, T., Kasamatsu, A., Miyamoto, I., Saito, T., Higo, M., Sakamoto, E.Y., Shiba, M., Tanzawa, H., & Uzawa, K. (2016). Overexpression of TMOD1 is associated with enhanced regional lymph node metastasis in human oral cancer. *International Journal of Oncology*, 48, 607-612. https://doi.org/10.3892/ijo.2015.3305

47. Jin, C., Chen, Z., Shi, W., & Lian, Q. (2019). Tropomodulin 3 promotes liver cancer progression by activating the MAPK/ERK signaling pathway. *Oncology Reports*, 41 (5), 3060-3068. https://doi.org/10.3892/or.2019.7052

48. Paul, D., Chanukuppa, V., Jaipal, P., Taunk, K., Adhav, R., Srivastava, S., Santra, K. M., & Rapole, S. (2016). Global proteomic profiling identifies etoposide chemoresistance markers in non-small cell lung carcinoma. *Journal of Proteomics*, *138*, 95–105. https://doi.org/10.1016/j.jprot.2016.02.008

49. Jiu, Y., Kumari, R., Fenix, A. M., Schaible, N., Liu, X., Varjosalo, M., Krishnan, R., Burnette, D. T., & Lappalainen, P. (2019). Myosin-18B Promotes the Assembly of Myosin II Stacks for Maturation of Contractile Actomyosin Bundles. *Current Biology*, *29*(1), 81-92.e5. https://doi.org/10.1016/j.cub.2018.11.045

50. Jiu, Y., Lehtimäki, J., Tojkander, S., Cheng, F., Jäälinoja, H., Liu, X., Varjosalo, M., Eriksson, E. J., & Lappalainen, P. (2015). Bidirectional interplay between vimentin intermediate filaments and contractile actin stress fibers. *Cell Reports*, *11*(10), 1511–1518. https://doi.org/10.1016/j.celrep.2015.05.008

51. Roux, K. J., Kim, D. I., Raida, M., & Burke, B. (2012). A promiscuous biotin ligase fusion protein identifies proximal and interacting proteins in mammalian cells. *Journal of Cell Biology*, *196*(6), 801–810. https://doi.org/10.1083/jcb.201112098
52. Ran, F. A., Hsu, P. D., Wright, J., Agarwala, V., Scott, D. A., & Zhang, F. (2013). Genome engineering using the CRISPR-Cas9 system. *Nature Protocols*, *8*, 2281. Retrieved from https://doi.org/10.1038/nprot.2013.143

53. Schneider, C. A., Rasband, W. S., & Eliceiri, K. W. (2012). NIH Image to ImageJ: 25 years of image analysis. *Nature Methods*, *9*(7), 671–675. https://www.ncbi.nlm.nih.gov/pubmed/22930834

54. Butler, J. P., Tolić-Nørrelykke, I. M., Fabry, B., & Fredberg, J. J. (2002). Traction fields, moments, and strain energy that cells exert on their surroundings. *American Journal of Physiology-Cell Physiology*, *282*(3), C595–C605. https://doi.org/10.1152/ajpcell.00270.2001

55. Krishnan, R., Park, C. Y., Lin, Y. C., Mead, J., Jaspers, R. T., Trepat, X., Lenormand, G., Tambe, D., Smolensky, V. A., Knoll, H. A., Butler, P. J., & Fredberg, J. J. (2009). Reinforcement versus fluidization in cytoskeletal mechanoresponsiveness. *PLoS ONE*, *4*(5). https://doi.org/10.1371/journal.pone.0005486

56. Ye, J., Coulouris, G., Zaretskaya, I., Cutcutache, I., Rozen, S., & Madden, T. L. (2012). Primer-BLAST: A tool to design target-specific primers for polymerase chain reaction. *BMC Bioinformatics, 13 (1), 134*. https://doi.org/10.1186/1471-2105-13-134

57. Pardee, J. D., Simpson, P. A., Stryer, L., & Spudich, J. A. (1982). Actin filaments undergo limited subunit exchange in physiological salt conditions. The Journal of Cell Biology, 94(2), 316 LP – 324. https://doi.org/10.1083/jcb.94.2.316

58. Smillie, L. B. (1982). Preparation and identification of α- and β-tropomyosins. In Structural and Contractile Proteins Part B: The Contractile Apparatus and the Cytoskeleton (Vol. 85, pp. 234–241). https://doi.org/https://doi.org/10.1016/0076-6879(82)85023-4

59. Schevzov, G., Whittaker, S., P., Fath, T., Lin, J., J., & Gunning, P., W. (2011). Tropomyosin isoforms and reagents. *Bioarchitecture, 1*(4), 135-164

FIGURE LEGENDS

Figure 1. Tmod1 and Tmod3 are components of contractile actin stress fibers. (**A**) Immunofluorescence images of U2OS cells, where the localization of endogenous Tmod3 and Tmod1 were detected by antibodies, and F-actin by phalloidin. Scale bar, 20 μm. (**B**) Localization of endogenous Tmod1 and Tmod3 in Tmod3 knockout cells (top) and Tmod1 siRNA cells (bottom). Scale bar, 20 μm. (**C**) Western blot analysis of Tmod3 and Tmod1 levels in lysates of wild-type (WT), Tmod3 knockout (Tmod3 KO), and Tmod1 siRNA U2OS cells. GAPDH was probed for equal sample loading. (**D**) Relative protein level of Tmod1, quantified by Western blot from WT and Tmod3 KO cell lysates. The Tmod1 level in wild-type cells was set to 1, and the data are presented as mean±S.E.M., n = 3 for WT and Tmod3 KO total cell lysates. (**E**) Relative protein level of Tmod3 in WT and Tmod 1 siRNA cell lysates. The Tmod3 level in wild-type was set to 1, and the data are presented as mean±S.E.M. n = 3 for wild-type and Tmod1 siRNA total cell lysates. Please note that depletion of either Tmod isoform resulted in upregulation of the other one.

Figure 2. Simultaneous depletion of Tmod1 and Tmod3 results in disruption of stress fibers, increased lamellipodia width, and impaired force generation. (**A**) Distribution of F-actin structures (detected by phalloidin) and focal adhesions (detected by vinculin antibody) in wild-type and Tmod3 KO +Tmod1 siRNA U2OS cells. Scale bar, 20 μm. (**B**) Stress fiber analysis of wild-type and Tmod3 KO + Tmod1 siRNA U2OS cells. Data are shown as mean±S.E.M., n (cells) = 78 wild-type, n = 67 Tmod3 KO + Tmod1 siRNA. The values obtained from Tmod3 KO + Tmod1 siRNA cells were compared to the ones from wild-type cells. ***P<0.001 (Student's *t*-test). (**C**) Quantification of the size distributions of focal adhesions. Data are shown as mean±S.E.M., n (cells) = 76 wild-type, n = 68 Tmod3 KO + Tmod1 siRNA. (**D**) Representative images of wild-type and Tmod3 KO +Tmod1 siRNA U2OS cells, where F-actin was detected by phalloidin and Arp2/3 complex by p34 antibody. Scale bar, 20 μm. Magnified regions of cell edges (corresponding to the white boxes) on the right show examples of F-actin and Arp2/3 -rich protrusions in wild-type and Tmod3 KO + Tmod1 siRNA cells. Scale bar, 5 μm. (**E**) Quantification of widths of Arp2/3-rich lamellipodial protrusions of wild-type and Tmod3 KO +Tmod1 siRNA U2OS cells. Data are shown as mean±S.E.M., n (cells) = 80 wild-type, n = 67 Tmod3 KO + Tmod1 siRNA. ***P<0.001 (Student's *t*-test). (**F**) Force maps of representative wild-type and Tmod3 KO + Tmod1 siRNA U2OS cells grown on 26 kPa polyacrylamide dishes with fluorescent nanobeads. (**G**) Quantification of traction forces in wild-type and Tmod3 KO + Tmod1 siRNA cells. The data are presented as mean±S.E.M.,

n = 41 for both wild-type and 43 for Tmod3 knockout + Tmod1 siRNA cells. **P<0.02 (Student's *t*-test).

Figure 3. Simultaneous depletion of Tmod1 and Tmod3 leads to a loss of tropomyosin-decorated actin filaments. (**A**) Representative immunofluorescence images of wild-type and Tmod3 KO + Tmod1 siRNA U2OS cells, where F-actin and tropomyosins (Tpm 2.1 and Tmp4.2) were detected by phalloidin and LC24 antibody, respectively. Scale bar, 20 μm. (**B**) Western blot analysis of Tpm1.6/1.7/2.1 (detected by TM311 antibody), Tpm2.1/4.2 (detected by LC24 antibody) and Tpm3.1/3.2 (detected by γ/9d antibody) in lysates of wild-type, Tmod3 KO, Tmod1 siRNA, and Tmod3 KO + Tmod1 siRNA cells. GAPDH was probed for equal sample loading. (**C**) Relative protein levels of tropomyosins quantified from wild-type, Tmod3 KO, Tmod1 siRNA, and Tmod3 KO + Tmod1 siRNA U2OS cell lysates. The protein levels in wild-type cells were set to 1. The data are presented as mean±S.E.M. n = 3 for wild-type, Tmod3 KO, Tmod1 siRNA and Tmod3 KO + Tmod1 siRNA U2OS cells.

Figure 4. Diminished tropomyosin levels and excessive lamellipodia formation, induced by the depletion of Tmods, can be rescued by expression of GFP-Tmod3. (**A**) Representative examples of Tmod3 KO + Tmod1 siRNA cells expressing GFP-Tmod3. F-actin was visualized by phalloidin, lamellipodia by cortactin antibodies, and Tpm2.1/4.2 by LC24 antibody. The Tmod3 KO + Tmod1 siRNA cells expressing GFP-Tmod3 are highlighted with white arrows. Scale bar, 20 μm. (**B**) Normalized relative total fluorescence intensities of Tpm2.1/4.2 (detected by LC24 antibody) quantified from immunofluorescence images of untransfected and GFP-Tmod3 expressing Tmod3 KO + Tmod1 siRNA cells from the same image, and the wild-type cells from a different set of images from an identical experiment. The values of wild-type cells were set to 1, and the data are presented as mean±S.E.M. n = 58 wild-type cells, and n = 46 cells from 21 images for both untransfected Tmod3 KO + Tmod1 siRNA cells and GFP-Tmod3 expressing Tmod3 KO + Tmod1 cells. The values obtained from the knockout and rescue cells were compared to the ones from wild-type cells. ***P<0.001 (Student's *t*-test) (**C**) Analysis of lamellipodia widths quantified from Arp2/3 immunofluorescence images of wild-type, Tmod3 KO + Tmod1 siRNA, and GFP-Tmod3 rescue cells. Data are presented as mean±S.E.M. n = 67 wild-type, n = 58 Tmod3 KO + Tmod1 siRNA cells, n = 48 GFP-Tmod3 rescue cells. The values obtained from knockout and rescue cells were compared to the ones from wild-type cells. ***P<0.001 (Student's *t*-test).

Figure 5. The tropomyosin-binding sites (TMBS) of Tmod3 are critical for its function *in vitro* and in cells. (A) Sequences of tropomyosin-binding sites 1 (TMBS1) and 2 (TMBS2) from human tropomodulin-3, colored by conservation score. Red boxes highlight the conserved leucine residues that were mutated to ablate tropomyosin binding. **(B - C)** Maximum polymerization rates (normalized to 0 nM Tmod control) of 1.5 μM (6% pyrene labeled) actin in the presence of 1.5 μM F-actin seeds, 25 nM CapZ, and various concentrations of either wild-type (WT) or TMBS mutant Tmod3 in the absence (B) or presence (C) of 1 μM tropomyosin. Each point represents mean ± S.E.M., n = 4 elongation curves. One star (*) indicates that zero difference in means fell outside the 95% credible interval, two stars (**) indicates that zero difference in means fell outside the 99% credible interval. (**D**) Representative images of Tmod3 KO + Tmod1 siRNA cells expressing GFP-Tmod3 (left) or GFP-Tmod3 TMBS mutant (right). F-actin was visualized by phalloidin, and focal adhesions by vinculin antibody. White arrows highlight the cells expressing GFP-Tmod3 constructs. Scale bar, 20 μm. **(E)** Stress fiber analysis (by Ridge detection plugin of Fiji ImageJ) from wild-type, Tmod3 KO + Tmod1 siRNA, GFP-Tmod3 rescued, and GFP-Tmod3 TMBS mutant rescued cells. Data are shown as mean±S.E.M. n (cells) = 79 wild-type, n = 71 Tmod3 KO + Tmod1 siRNA, n = 48 GFP-Tmod3 rescue, n = 45 GFP-Tmod3 TMBS mutant rescue. The values obtained from knockout/knockdown and rescue cells were compared to the ones from wild-type cells. N.S. (not significant), *P<0.05, **P<0.02, ***P<0.001 (Student's *t*-test). (**F**) Relative protein levels of tropomyosins quantified from wild-type, GFP-Tmod3 rescue, Tmod3 KO + Tmod1 siRNA and GFP-Tmod3 TMBS mutant rescue U2OS cell lysates. The protein levels in wild-type cells were set to 1. The data are presented as mean±S.E.M. n = 3 for wild-type, GFP-Tmod3 rescue, Tmod3 KO + Tmod1 siRNA, and GFP-Tmod3 TMBS mutant rescue U2OS cells.

Figure 6. Tmods antagonize with the Arp2/3 complex in stabilizing tropomyosin-decorated actin stress fibers. (**A**) Representative examples of Tmod3 KO + Tmod1 siRNA cells treated with DMSO, or 100 μM CK666, or in which the ARPC2 subunit of the Arp2/3 complex was depleted by siRNA. F-actin was detected by phalloidin and focal adhesions and Arp2/3 complex by vinculin and p34 antibodies, respectively. Scale bar, 20 μm. Please note the re-appearance of stress fibers and an increase in the size of focal adhesions in Tmod knockout/knockdown cells after treatment with the Arp2/3 complex inhibitor or following siRNA depletion of the functional Arp2/3 complex. (**B**) Analysis of cell circularity index of wild-type cells, Tmod3 KO + Tmod1 siRNA cells and Tmod3 KO + Tmod1 siRNA treated with CK666. The values obtained from untreated and CK666-treated

knockout/knockdown cells were compared to the ones from wild-type cells, and the data are shown as mean±S.E.M., n (cells) = 80 wild-type, n = 72 Tmod3 KO + Tmod1 siRNA, n = 72 Tmod3 KO + Tmod1 siRNA + CK666. N.S. (not significant), ***P<0.001 (Student's *t*-test). (**C**) Size distributions of focal adhesions in wild-type cells, Tmod3 KO + Tmod1 siRNA cells, and CK666 treated Tmod3 KO + Tmod1 siRNA cells. Data were obtained and analyzed as in Fig. 2C, and presented as mean±S.E.M., n (cells) = 62 wild-type, n = 64 Tmod3 KO + Tmod1 siRNA, n = 67 Tmod3 KO + Tmod1 siRNA + CK666. (**D**) Stress fibers analysis (by Ridge detection plugin of Fiji ImageJ) from wild-type cells, Tmod3 KO + Tmod1 siRNA cells, CK666 treated Tmod3 KO + Tmod1 siRNA cells, and ARPC2 siRNA + Tmod3 KO + Tmod1 siRNA cells. Data are shown as mean±S.E.M. The values obtained from untreated, CK666-treated, and ARPC2 depleted knockout/knockdown cells were compared to the ones from wild-type cells. n (cells) = 73 wild-type, n = 69 Tmod3 KO + Tmod1 siRNA, n = 58 Tmod3 KO + Tmod1 siRNA + CK666, n = 55 Tmod3 KO + Tmod1 siRNA + ARPC2 siRNA. N.S. (not significant), *P<0.05, **P<0.02, ***P<0.001 (Student's *t*-test). (**E**) Relative protein levels of tropomyosins quantified from wild-type, Tmod3 KO + Tmod1 siRNA, CK666 treated Tmod3 KO + Tmod1 siRNA cells, and ARPC2 siRNA + Tmod3 KO + Tmod1 siRNA U2OS cell lysates. The protein levels in wild-type cells were set to 1. The data are presented as mean±S.E.M. n = 3 for wild-type, Tmod3 KO + Tmod1 siRNA, CK666 treated Tmod3 KO + Tmod1 siRNA cells, and ARPC2 siRNA + Tmod3 KO + Tmod1 siRNA U2OS cells.

Figure 7. A working model for the role of Tmods in stabilizing tropomyosin-actin filaments, and hence maintaining the homeostasis between Arp2/3 complex-nucleated protrusive and tropomyosin-decorated contractile actin filament pools in cells. (**A**) Actin filaments that are polymerized by formins, and decorated by tropomyosins are stabilized through pointed-end capping by Tmods (left). In the absence of Tmods these filaments become unstable (right). (**B**) Depletion of Tmods results in disruption of tropomyosin-decorated actin filaments, and consequent increase in the Arp2/3-nucleated actin filament networks. (**C**) This unbalance in actin filament homeostasis results in the loss of stress fibers, and consequent decrease in force generation.

Figure 1

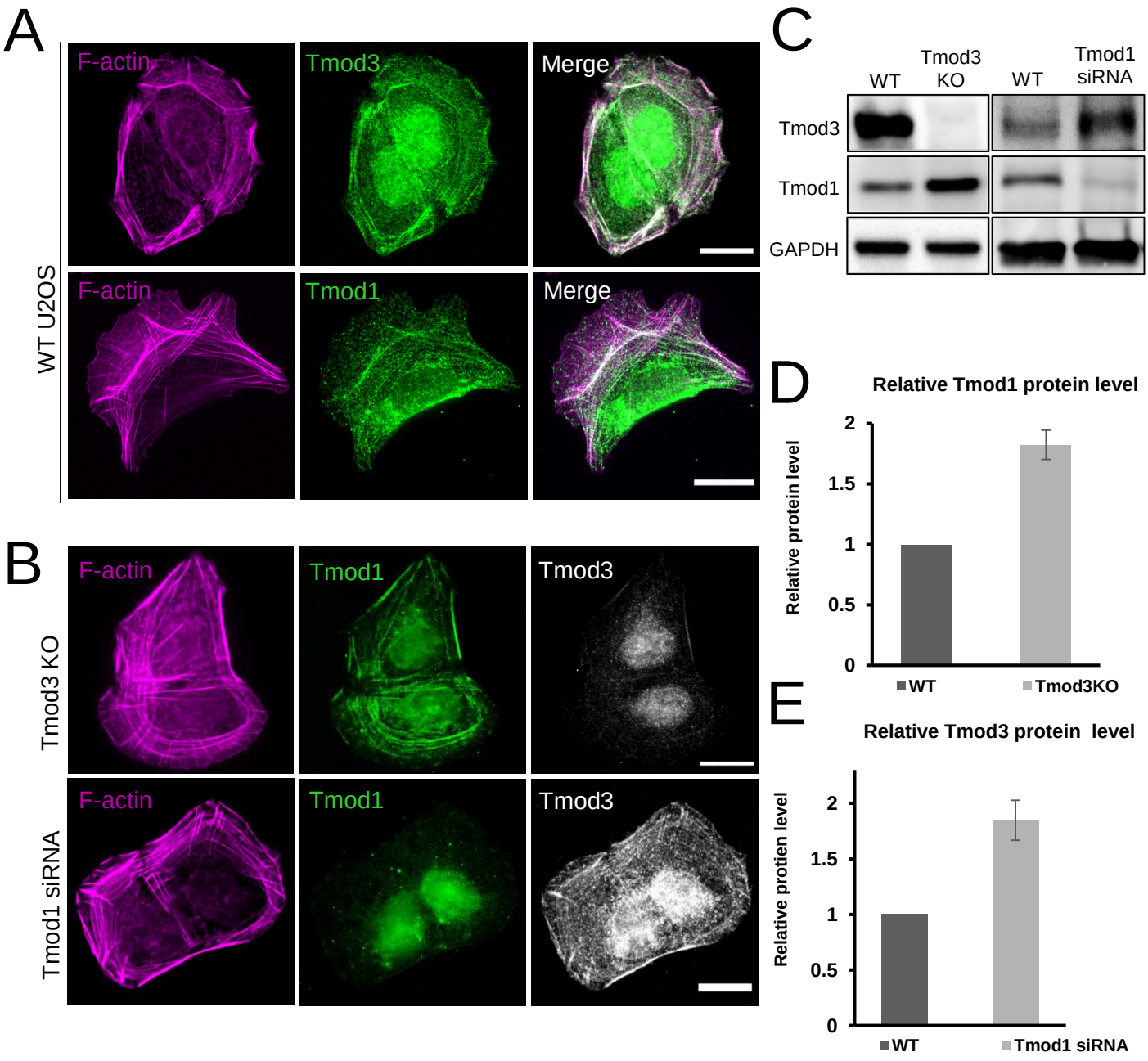
A
F-actin
Tmod3
Merge
F-actin
Tmod1
Merge
WT U2OS
B
F-actin
Tmod1
Tmod3
Tmod3 KO
F-actin
Tmod1
Tmod3
Tmod1 siRNA
C
WT
Tmod3 KO
WT
Tmod1 siRNA
Tmod3
Tmod1
GAPDH
D
Relative Tmod1 protein level
Relative protein level
2
1.5
1
0.5
0
WT
Tmod3KO
E
Relative Tmod3 protein level
Relative protien level
2
1.5
1
0.5
0
WT
Tmod1 siRNA

Figure 2

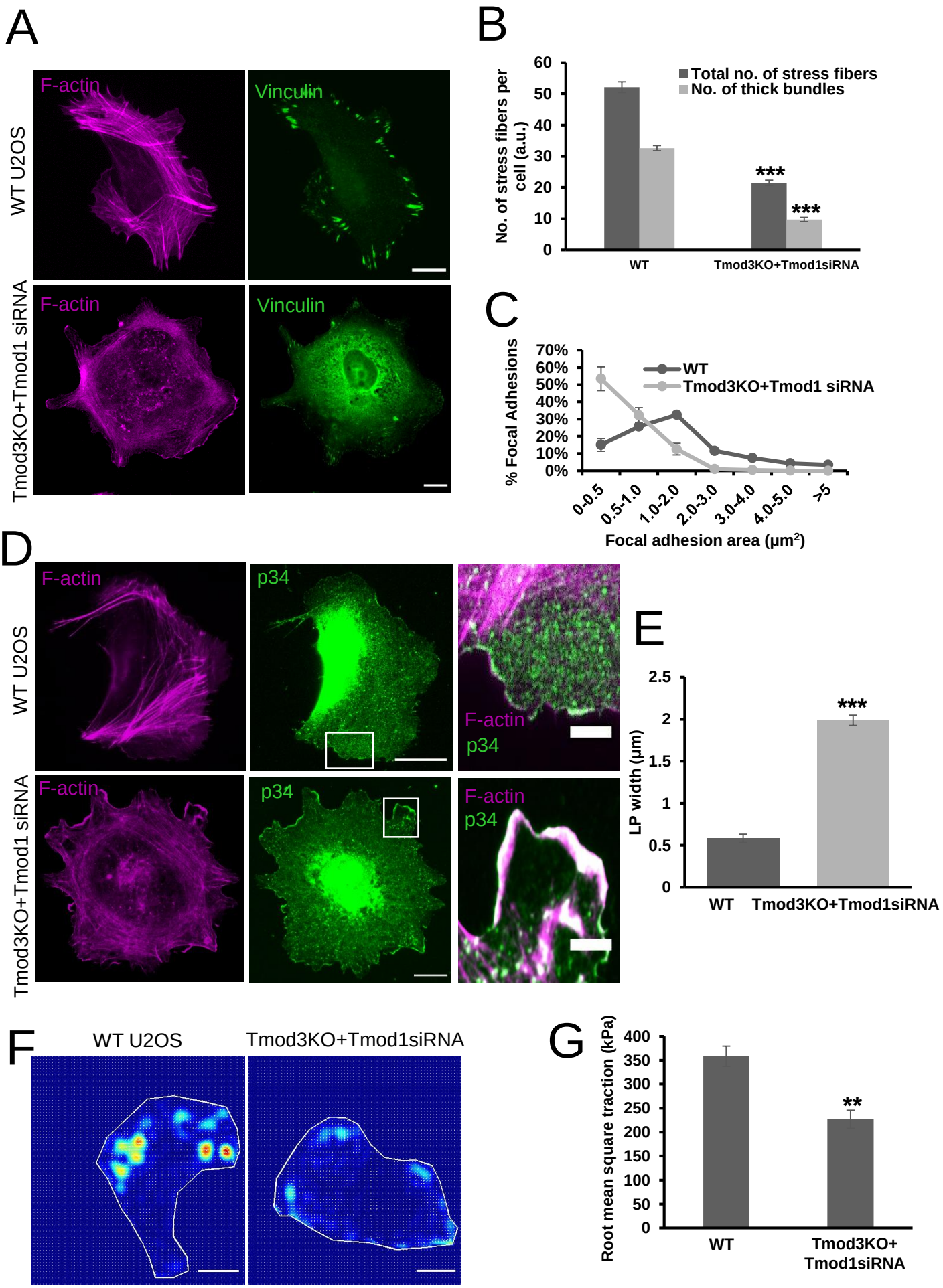
A
WT U2OS
Tmod3KO+Tmod1 siRNA
F-actin
Vinculin
B
No. of stress fibers per cell (a.u.)
Total no. of stress fibers
No. of thick bundles
***
***
WT
Tmod3KO+Tmod1siRNA
C
% Focal Adhesions
WT
Tmod3KO+Tmod1 siRNA
0-0.5
0.5-1.0
1.0-2.0
2.0-3.0
3.0-4.0
4.0-5.0
>5
Focal adhesion area (μm²)
D
WT U2OS
Tmod3KO+Tmod1 siRNA
F-actin
p34
E
LP width (μm)
***
WT
Tmod3KO+Tmod1siRNA
F
WT U2OS
Tmod3KO+Tmod1siRNA
G
Root mean square traction (kPa)
**
WT
Tmod3KO+
Tmod1siRNA

Figure 3

A

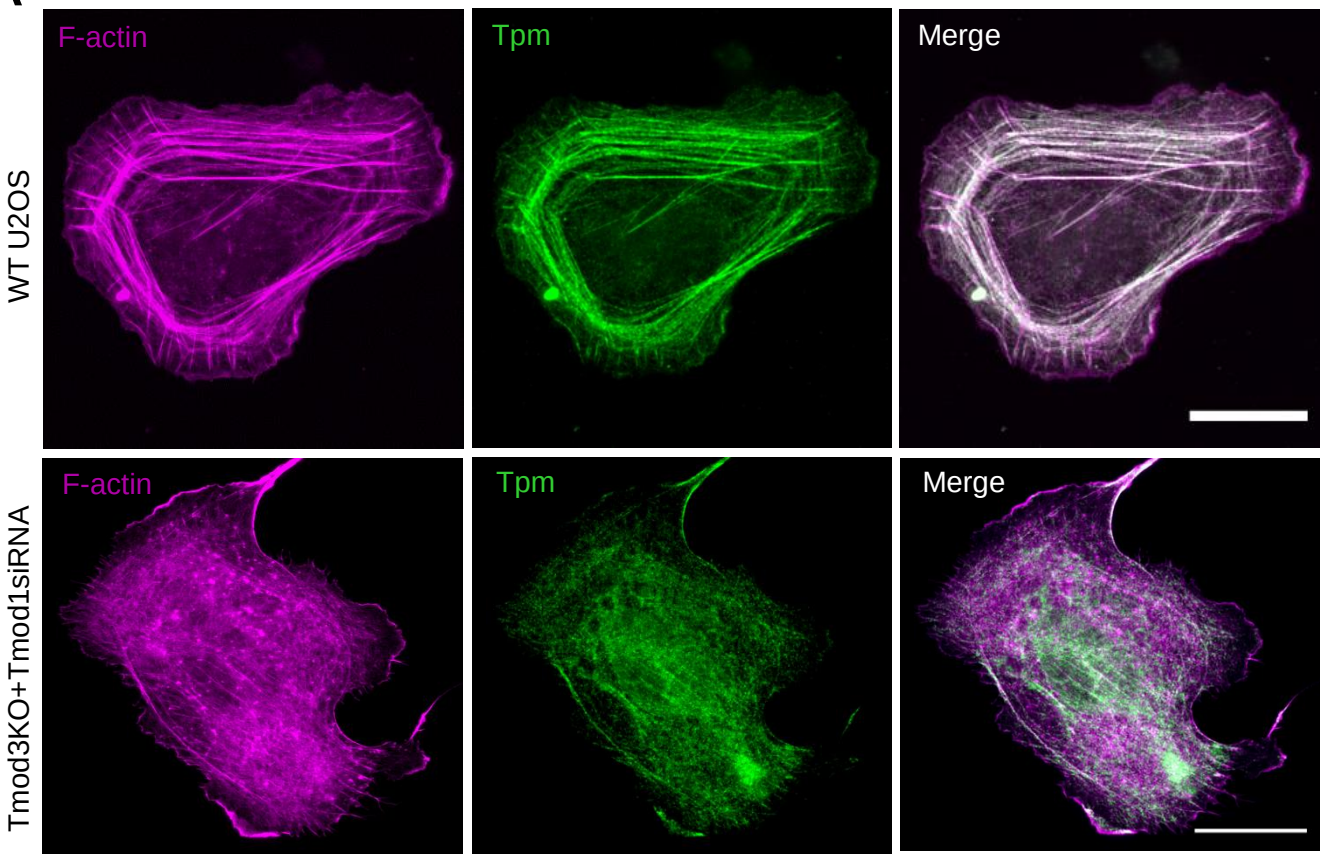
F-actin
Tpm
Merge
WT U2OS
F-actin
Tpm
Merge
Tmod3KO+Tmod1siRNA

B

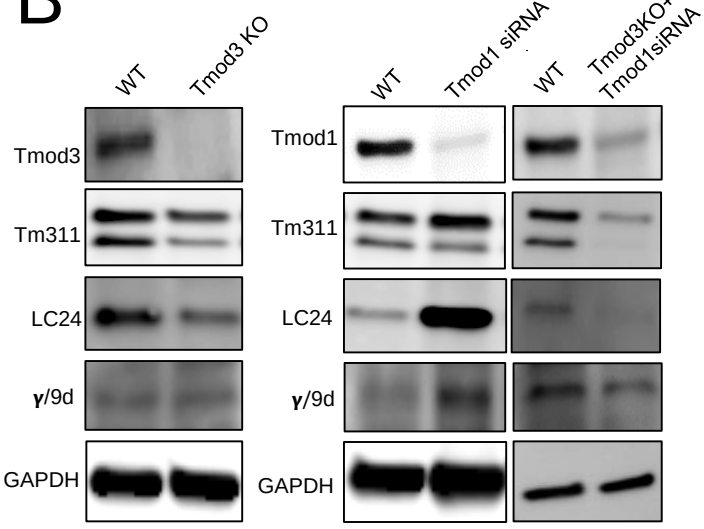
WT
Tmod3 KO
Tmod3
Tm311
LC24
γ/9d
GAPDH
WT
Tmod1 siRNA
WT
Tmod3KO+
Tmod1siRNA
Tmod1
Tm311
LC24
γ/9d
GAPDH

C

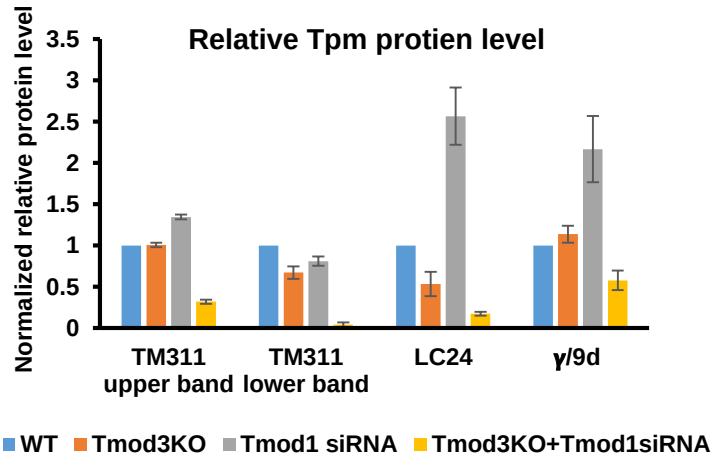
Relative Tpm protien level
Normalized relative protein level
3.5
3
2.5
2
1.5
1
0.5
0
TM311
upper band
TM311
lower band
LC24
γ/9d
WT
Tmod3KO
Tmod1 siRNA
Tmod3KO+Tmod1siRNA

Figure 4

A

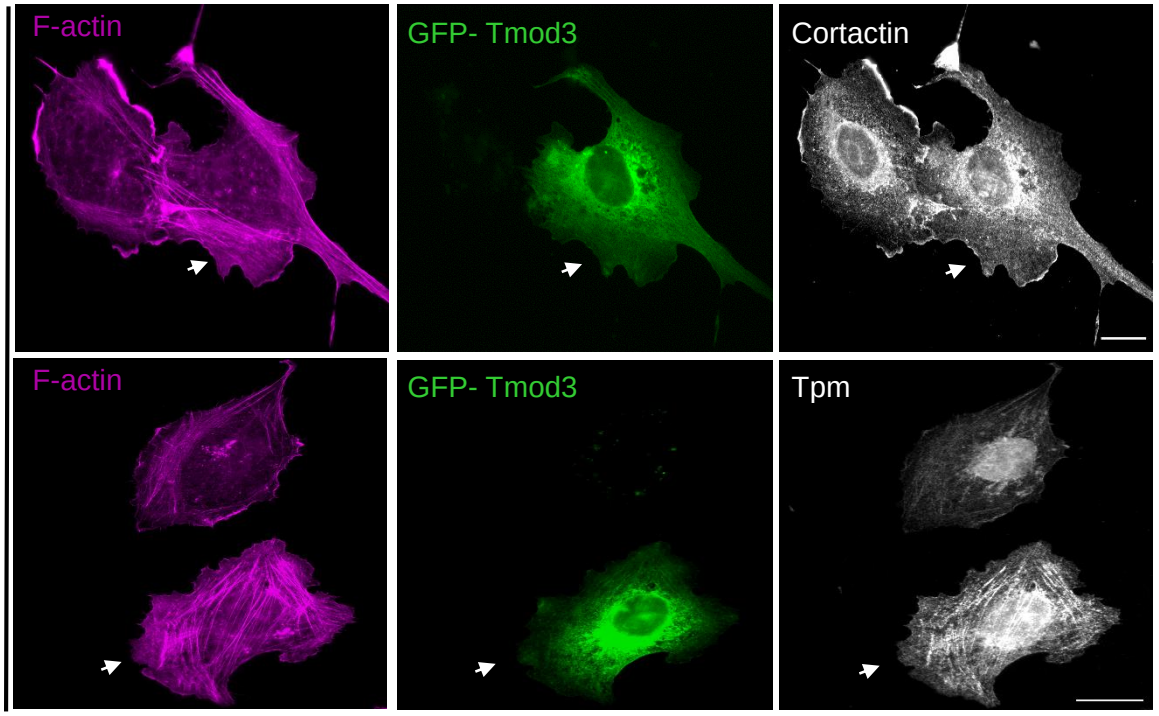
F-actin
GFP- Tmod3
Cortactin
Tmod3KO+Tmod1siRNA
F-actin
GFP- Tmod3
Tpm

B

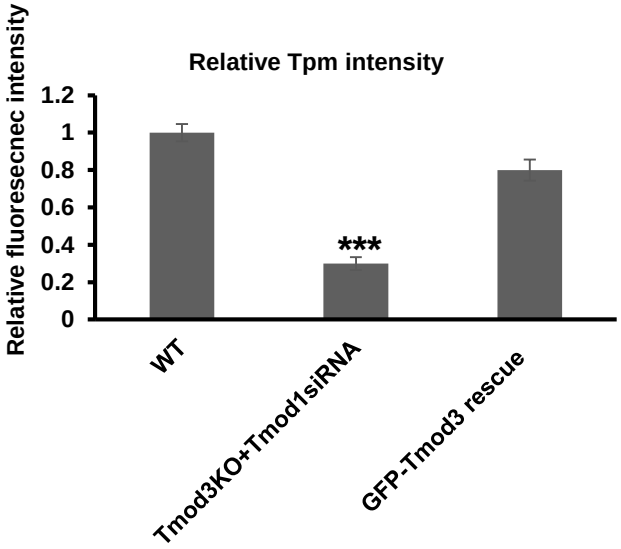
Relative Tpm intensity
Relative fluorescnec intensity
1.2
1
0.8
0.6
0.4
0.2
0
***
WT
Tmod3KO+Tmod1siRNA
GFP-Tmod3 rescue

C

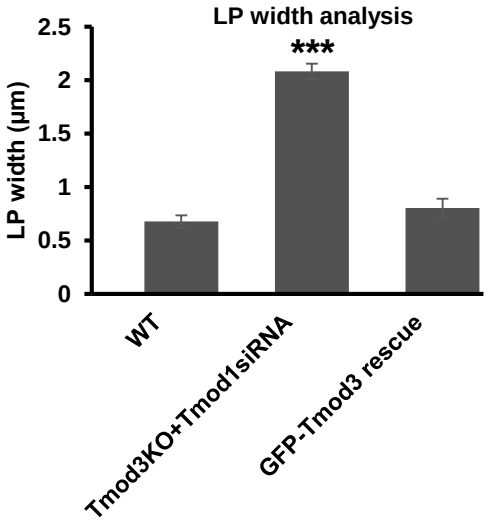
LP width analysis
LP width (µm)
2.5
2
1.5
1
0.5
0
***
WT
Tmod3KO+Tmod1siRNA
GFP-Tmod3 rescue

Figure 5

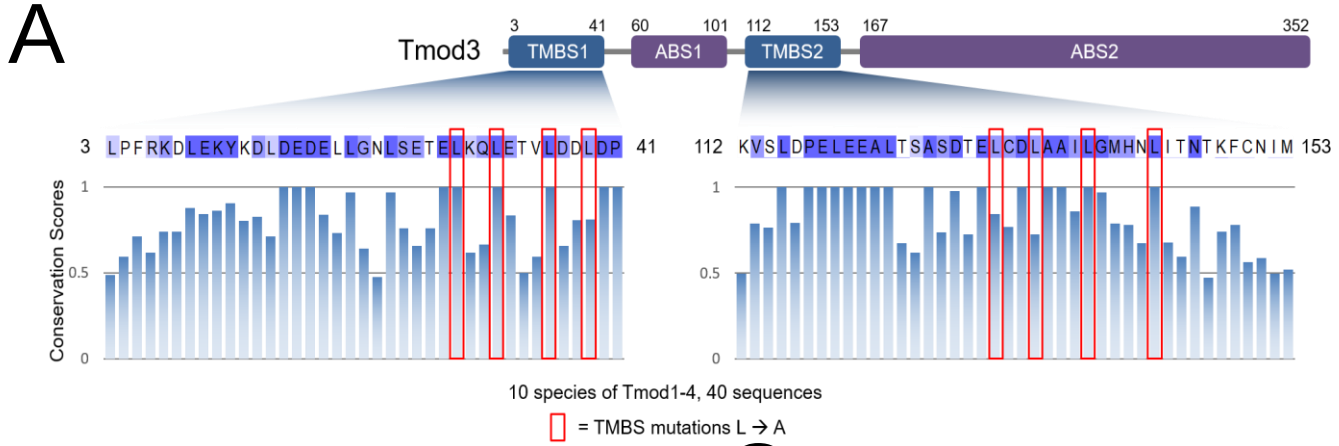
A
Tmod3
3
41
60
101
112
153
167
352
TMBS1
ABS1
TMBS2
ABS2
3 LPFRKDLEKYKDLDEDELLGNLSETELKQLETVLDDLDP 41
112 KVSLDPELEEALTSASDTELCDLAAILGMHNLITNTKFCNIM 153
Conservation Scores
1
0.5
0
10 species of Tmod1-4, 40 sequences
= TMBS mutations L → A

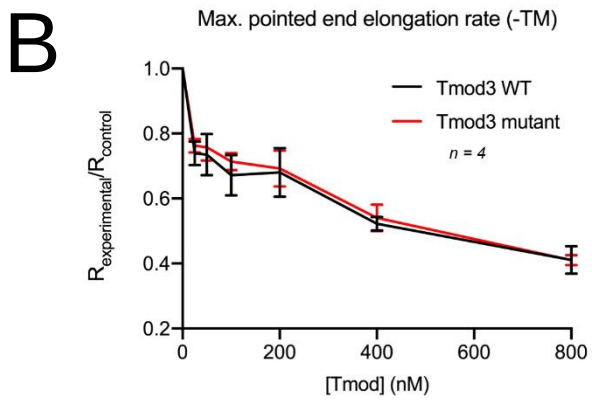
B
Max. pointed end elongation rate (-TM)
Tmod3 WT
Tmod3 mutant
n = 4
R experimental/R control
1.0
0.8
0.6
0.4
0.2
0
200
400
600
800
[Tmod] (nM)

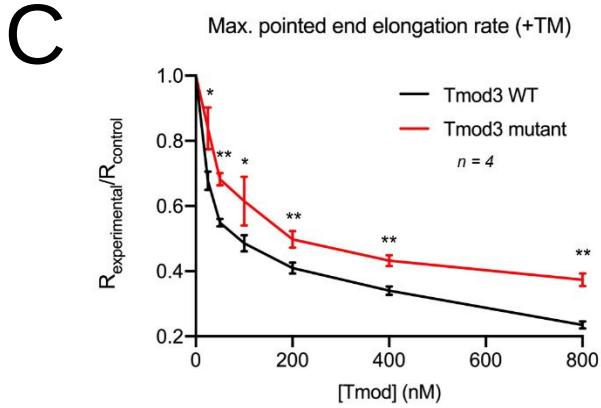
C
Max. pointed end elongation rate (+TM)
Tmod3 WT
Tmod3 mutant
n = 4
R experimental/R control
1.0
0.8
0.6
0.4
0.2
0
200
400
600
800
[Tmod] (nM)
*
**
*
**
**
**

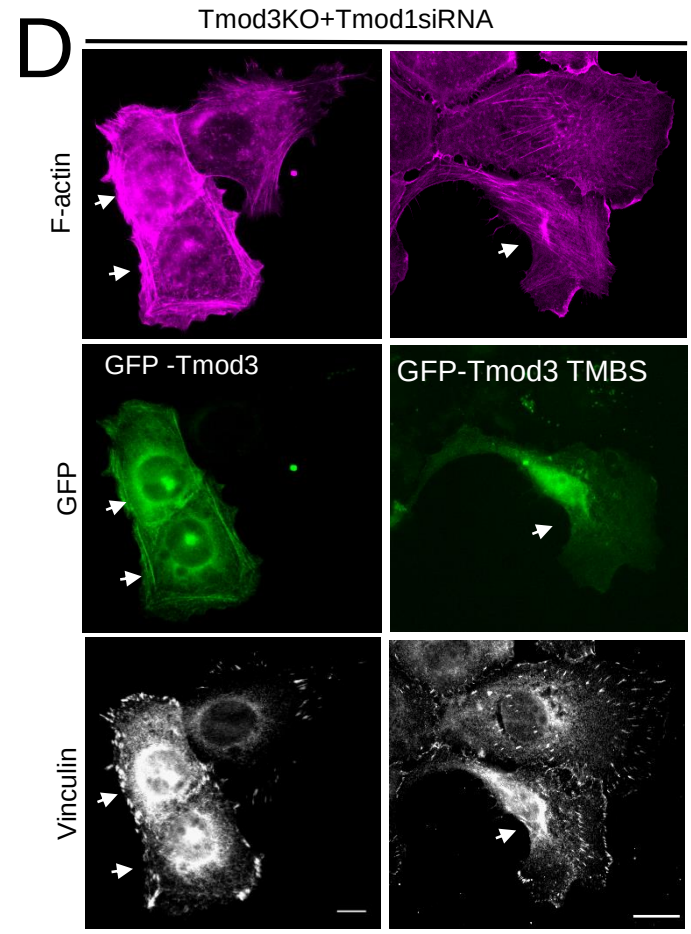
D
Tmod3KO+Tmod1siRNA
F-actin
GFP
GFP -Tmod3
GFP-Tmod3 TMBS
Vinculin

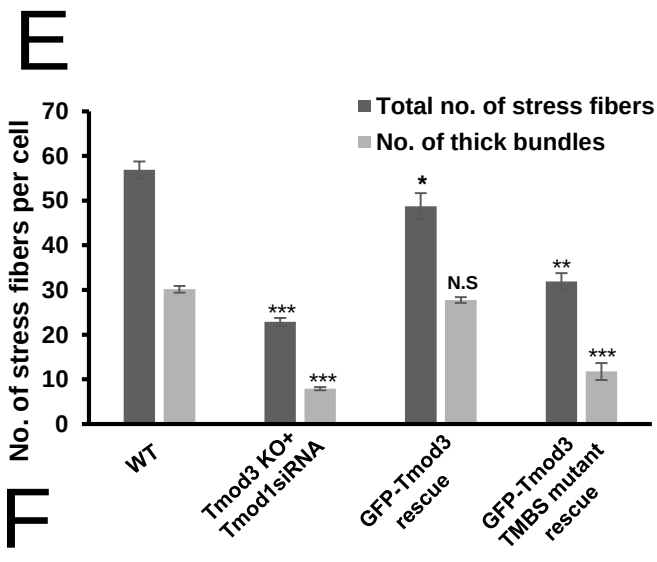
E
Total no. of stress fibers
No. of thick bundles
No. of stress fibers per cell
70
60
50
40
30
20
10
0
***
***
*
N.S
**
***
WT
Tmod3 KO+ Tmod1siRNA
GFP-Tmod3 rescue
GFP-Tmod3 TMBS mutant rescue

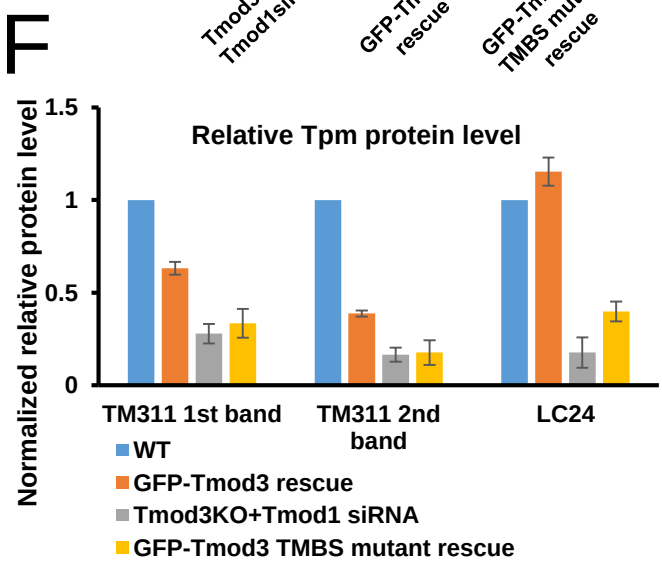
F
Relative Tpm protein level
Normalized relative protein level
1.5
1
0.5
0
TM311 1st band
TM311 2nd band
LC24
WT
GFP-Tmod3 rescue
Tmod3KO+Tmod1 siRNA
GFP-Tmod3 TMBS mutant rescue

Figure 6

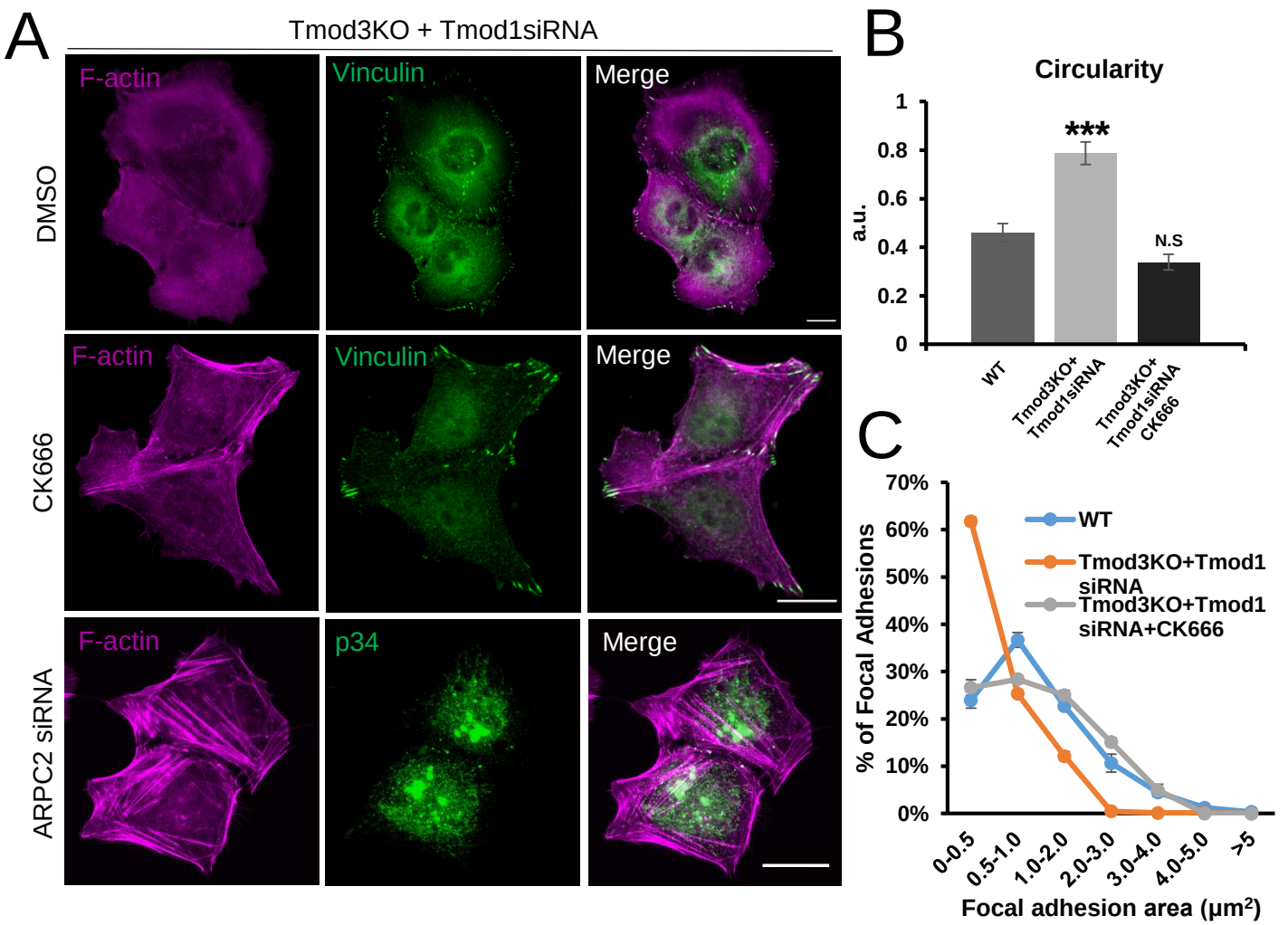
A
Tmod3KO + Tmod1siRNA
F-actin
Vinculin
Merge
DMSO
CK666
ARPC2 siRNA
p34
B
Circularity
a.u.
***
N.S
WT
Tmod3KO+ Tmod1siRNA
Tmod3KO+ Tmod1siRNA CK666
C
% of Focal Adhesions
WT
Tmod3KO+Tmod1 siRNA
Tmod3KO+Tmod1 siRNA+CK666
0-0.5
0.5-1.0
1.0-2.0
2.0-3.0
3.0-4.0
4.0-5.0
>5
Focal adhesion area (μm²)
D
No. of stress fibers per cell (a.u.)
N.S
Tmod3KO+ Tmod1+ ARPC2 siRNA
Total no. of stress fibers
No. of thick bundles
E
Relative Tpm protein level
Normalized relative protein level
TM311 1st band
TM311 2nd band
LC24
Tmod3KO+Tmod1 siRNA+ ARPC2 siRNA

Figure 7

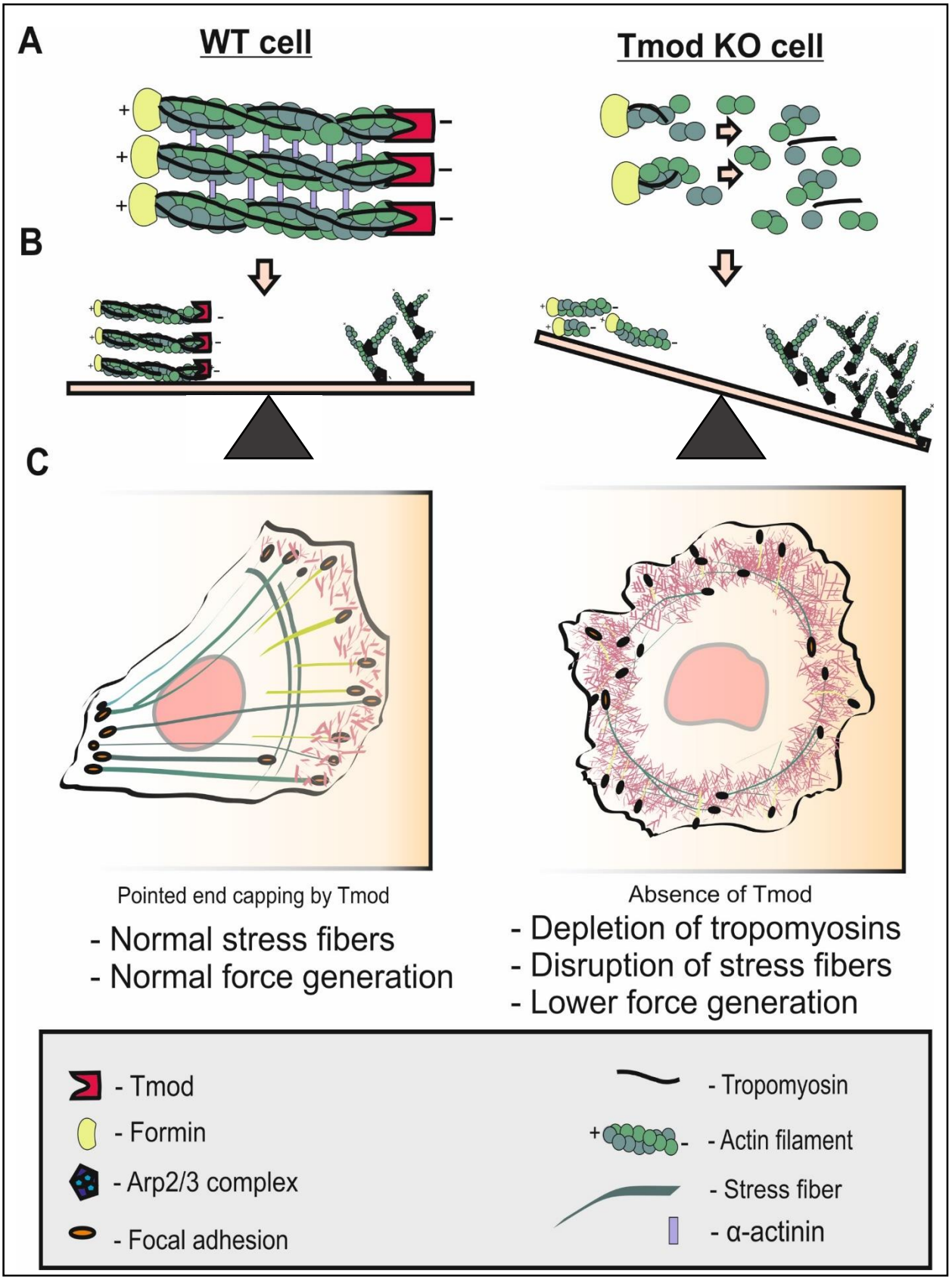
A
WT cell
Tmod KO cell
B
C
Pointed end capping by Tmod
- Normal stress fibers
- Normal force generation
Absence of Tmod
- Depletion of tropomyosins
- Disruption of stress fibers
- Lower force generation
- Tmod
- Formin
- Arp2/3 complex
- Focal adhesion
- Tropomyosin
- Actin filament
- Stress fiber
- α-actinin

Figure S1

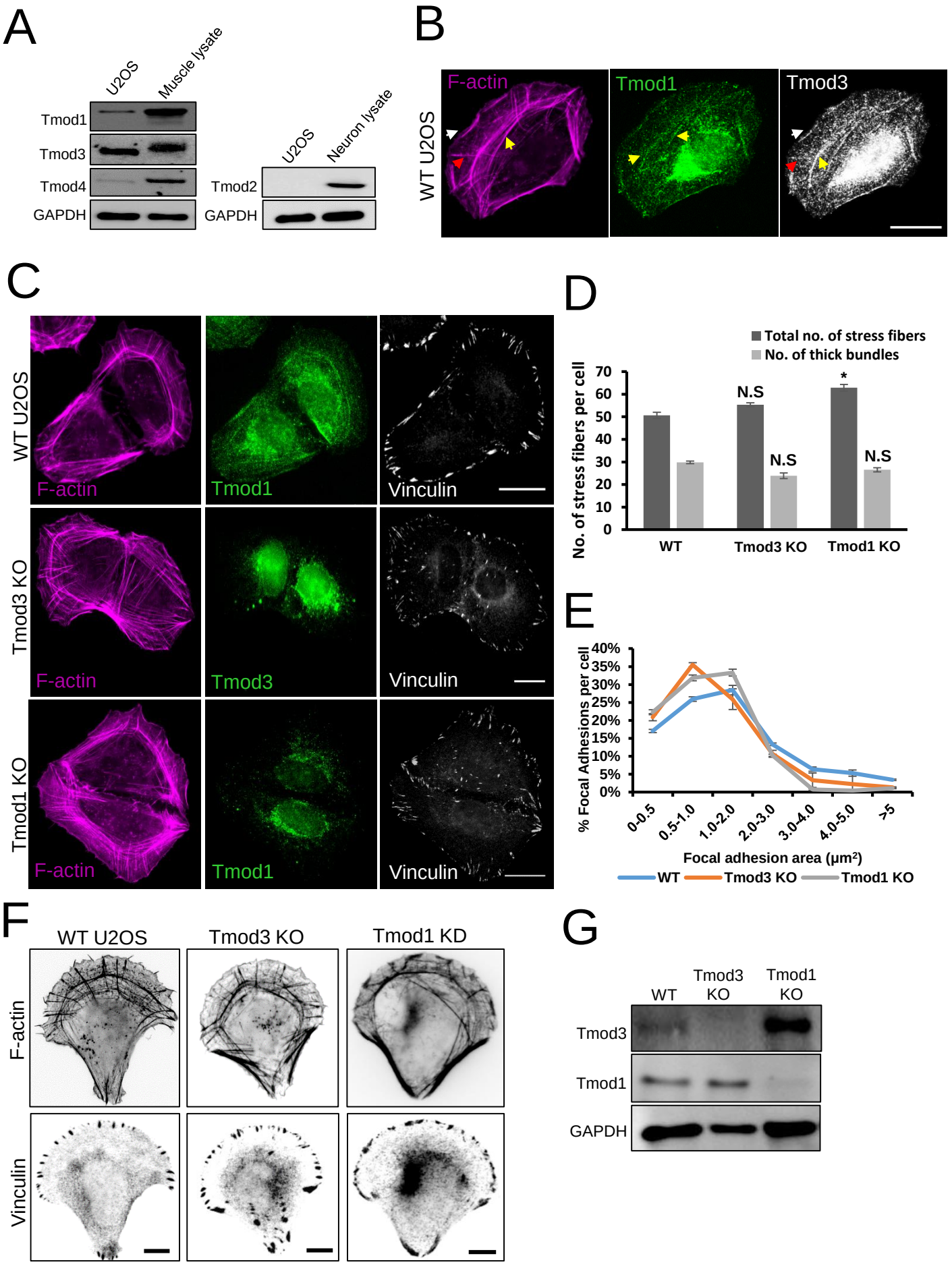
A
U2OS
Muscle lysate
Tmod1
Tmod3
Tmod4
GAPDH
U2OS
Neuron lysate
Tmod2
GAPDH
B
WT U2OS
F-actin
Tmod1
Tmod3
C
WT U2OS
F-actin
Tmod1
Vinculin
Tmod3 KO
F-actin
Tmod3
Vinculin
Tmod1 KO
F-actin
Tmod1
Vinculin
D
Total no. of stress fibers
No. of thick bundles
No. of stress fibers per cell
70
60
50
40
30
20
10
0
N.S
N.S
*
N.S
WT
Tmod3 KO
Tmod1 KO
E
% Focal Adhesions per cell
40%
35%
30%
25%
20%
15%
10%
5%
0%
0-0.5
0.5-1.0
1.0-2.0
2.0-3.0
3.0-4.0
4.0-5.0
>5
Focal adhesion area (μm²)
WT
Tmod3 KO
Tmod1 KO
F
WT U2OS
Tmod3 KO
Tmod1 KD
F-actin
Vinculin
G
WT
Tmod3 KO
Tmod1 KO
Tmod3
Tmod1
GAPDH

Figure S2

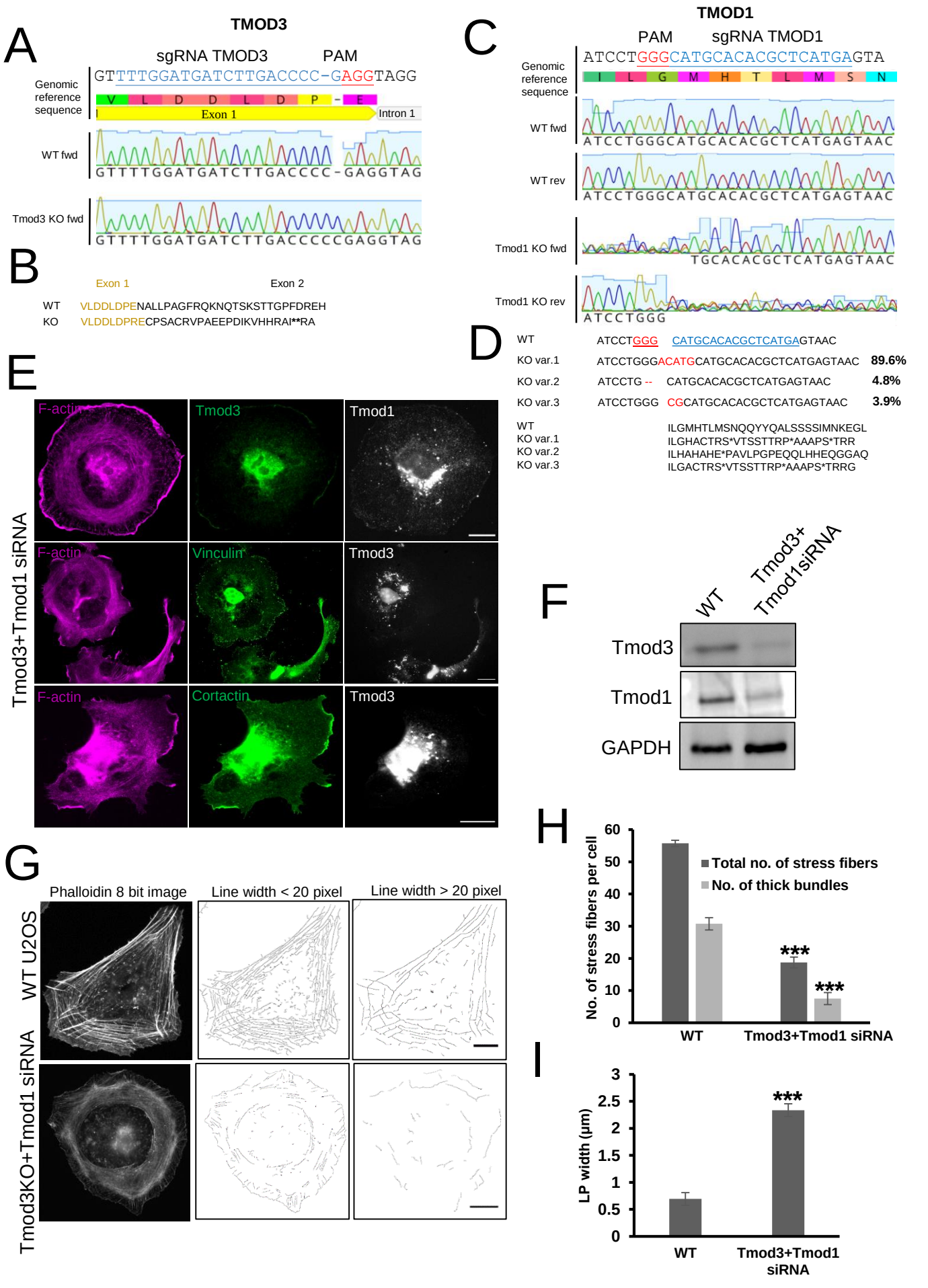
A
TMOD3
sgRNA TMOD3
PAM
GTTTTGGATGATCTTGACCCC-GAGGTAGG
Genomic reference sequence
V L D D L D P - E
Exon 1
Intron 1
WT fwd
GTTTTGGATGATCTTGACCCC-GAGGTAG
Tmod3 KO fwd
GTTTTGGATGATCTTGACCCCCGAGGTAG
B
Exon 1
Exon 2
WT VLDDLDPENALLPAGFRQKNQTSKSTTGPFDREH
KO VLDDLDPRECPSACRVPAEEPDIKVHHRAI**RA
C
TMOD1
PAM
sgRNA TMOD1
ATCCTGGGCATGCACACGCTCATGAGTA
Genomic reference sequence
I L G M H T L M S N
WT fwd
ATCCTGGGCATGCACACGCTCATGAGTAAC
WT rev
ATCCTGGGCATGCACACGCTCATGAGTAAC
Tmod1 KO fwd
TGCACACGCTCATGAGTAAC
Tmod1 KO rev
ATCCTGGG
D
WT ATCCTGGG CATGCACACGCTCATGAGTAAC
KO var.1 ATCCTGGGACATGCATGCACACGCTCATGAGTAAC 89.6%
KO var.2 ATCCTG -- CATGCACACGCTCATGAGTAAC 4.8%
KO var.3 ATCCTGGG CGCATGCACACGCTCATGAGTAAC 3.9%
WT ILGMHTLMSNQQYYQALSSSSIMNKEGL
KO var.1 ILGHACTRS*VTSSTTRP*AAAPS*TRR
KO var.2 ILHAHAHE*PAVLPGPEQQLHHEQGGAQ
KO var.3 ILGACTRS*VTSSTTRP*AAAPS*TRRG
E
F-actin
Tmod3
Tmod1
Tmod3+Tmod1 siRNA
F-actin
Vinculin
Tmod3
F-actin
Cortactin
Tmod3
F
WT
Tmod3+ Tmod1siRNA
Tmod3
Tmod1
GAPDH
G
Phalloidin 8 bit image
Line width < 20 pixel
Line width > 20 pixel
WT U2OS
Tmod3KO+Tmod1 siRNA
H
No. of stress fibers per cell
60
50
40
30
20
10
0
Total no. of stress fibers
No. of thick bundles
***
***
WT
Tmod3+Tmod1 siRNA
I
LP width (µm)
3
2.5
2
1.5
1
0.5
0
***
WT
Tmod3+Tmod1 siRNA

Figure S3

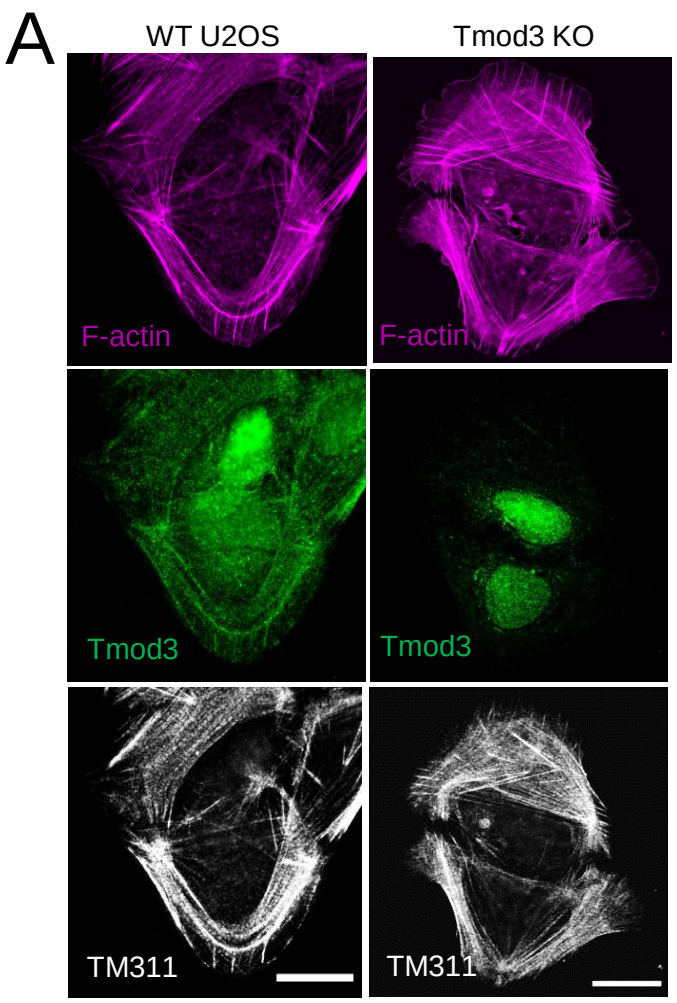
A
WT U2OS
Tmod3 KO
F-actin
F-actin
Tmod3
Tmod3
TM311
TM311

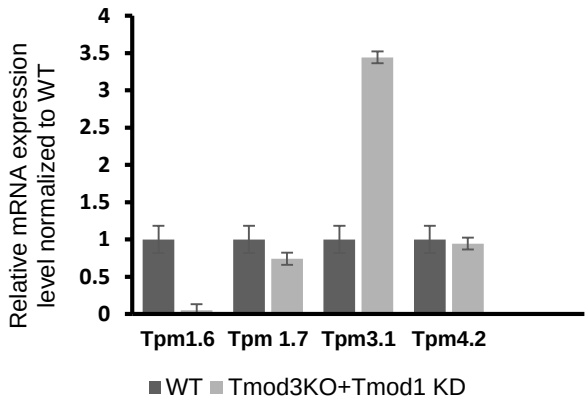
B
Relative mRNA expression level normalized to WT
4
3.5
3
2.5
2
1.5
1
0.5
0
Tpm1.6
Tpm 1.7
Tpm3.1
Tpm4.2
WT
Tmod3KO+Tmod1 KD

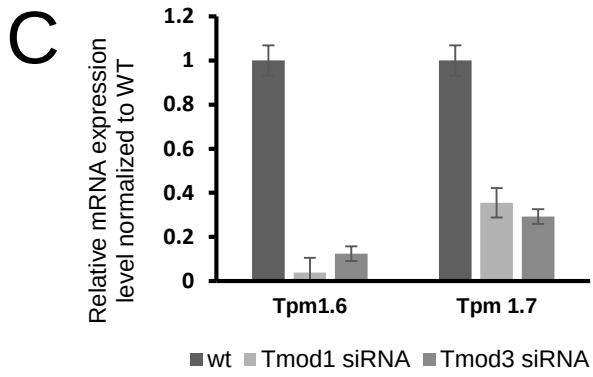
C
Relative mRNA expression level normalized to WT
1.2
1
0.8
0.6
0.4
0.2
0
Tpm1.6
Tpm 1.7
wt
Tmod1 siRNA
Tmod3 siRNA

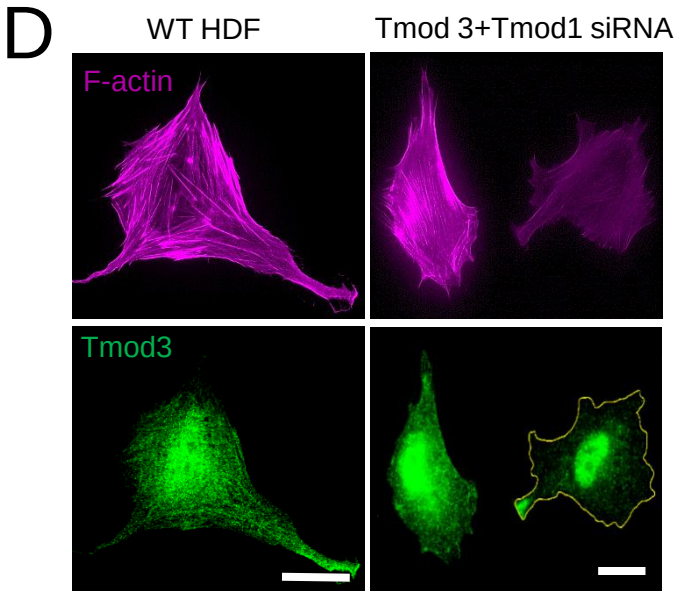
D
WT HDF
Tmod 3+Tmod1 siRNA
F-actin
Tmod3

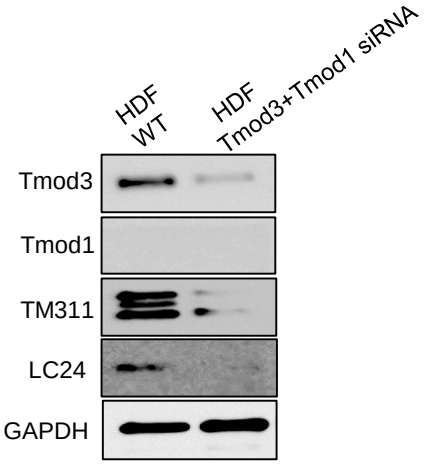
E
HDF WT
HDF Tmod3+Tmod1 siRNA
Tmod3
Tmod1
TM311
LC24
GAPDH

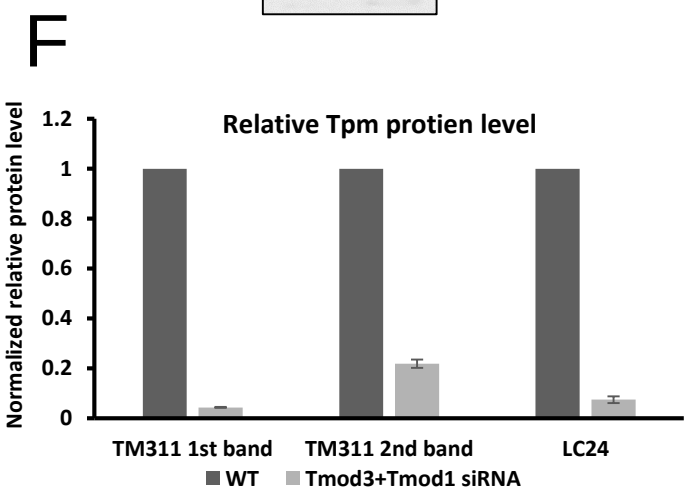
F
Relative Tpm protien level
Normalized relative protein level
1.2
1
0.8
0.6
0.4
0.2
0
TM311 1st band
TM311 2nd band
LC24
WT
Tmod3+Tmod1 siRNA

Figure S4

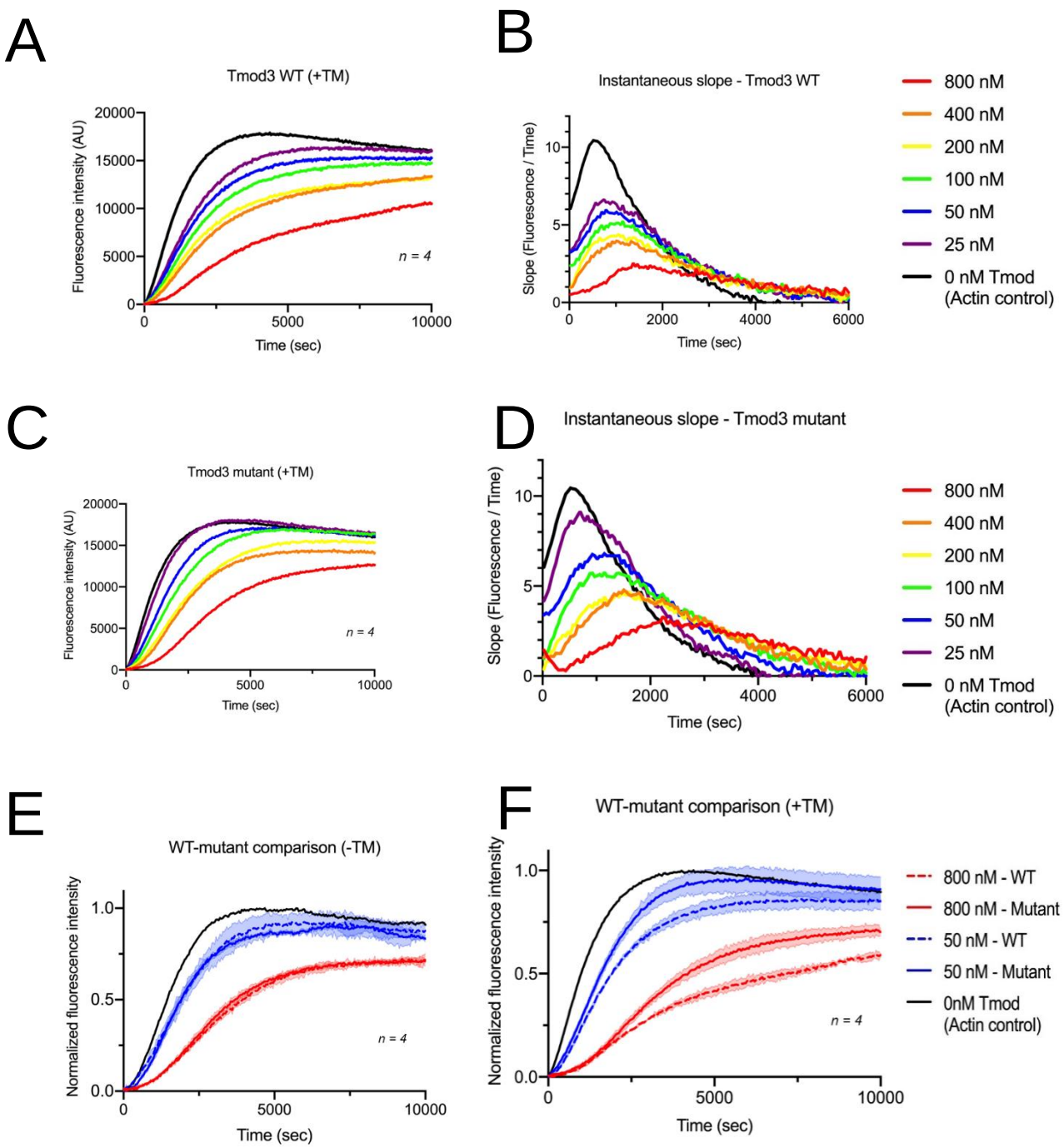
A
Tmod3 WT (+TM)
Fluorescence intensity (AU)
20000
15000
10000
5000
0
0
5000
10000
Time (sec)
n = 4
B
Instantaneous slope - Tmod3 WT
Slope (Fluorescence / Time)
10
5
0
0
2000
4000
6000
Time (sec)
800 nM
400 nM
200 nM
100 nM
50 nM
25 nM
0 nM Tmod
(Actin control)
C
Tmod3 mutant (+TM)
Fluorescence intensity (AU)
20000
15000
10000
5000
0
0
5000
10000
Time (sec)
n = 4
D
Instantaneous slope - Tmod3 mutant
Slope (Fluorescence / Time)
10
5
0
0
2000
4000
6000
Time (sec)
800 nM
400 nM
200 nM
100 nM
50 nM
25 nM
0 nM Tmod
(Actin control)
E
WT-mutant comparison (-TM)
Normalized fluorescence intensity
1.0
0.5
0.0
0
5000
10000
Time (sec)
n = 4
F
WT-mutant comparison (+TM)
Normalized fluorescence intensity
1.0
0.5
0.0
0
5000
10000
Time (sec)
n = 4
800 nM - WT
800 nM - Mutant
50 nM - WT
50 nM - Mutant
0nM Tmod
(Actin control)

Figure S5

A

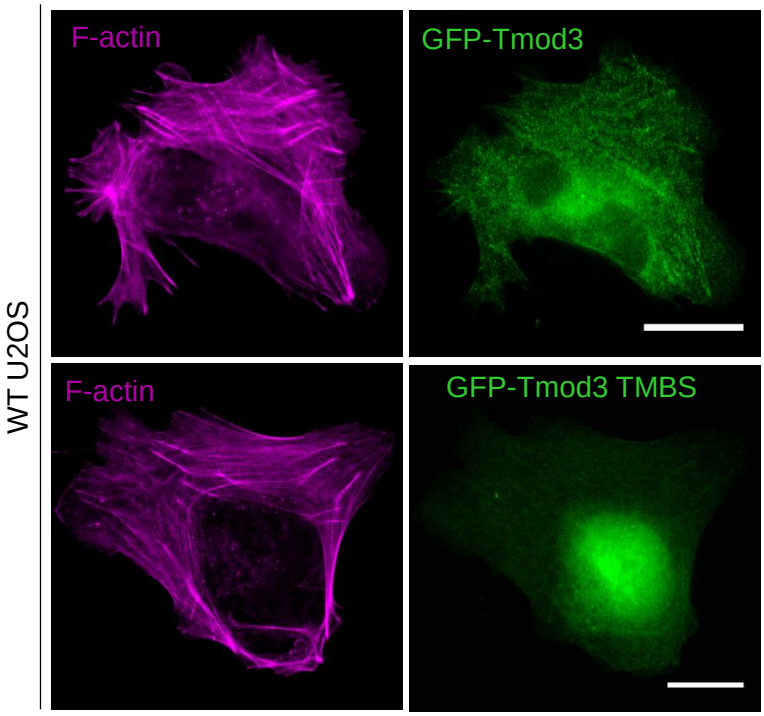

B

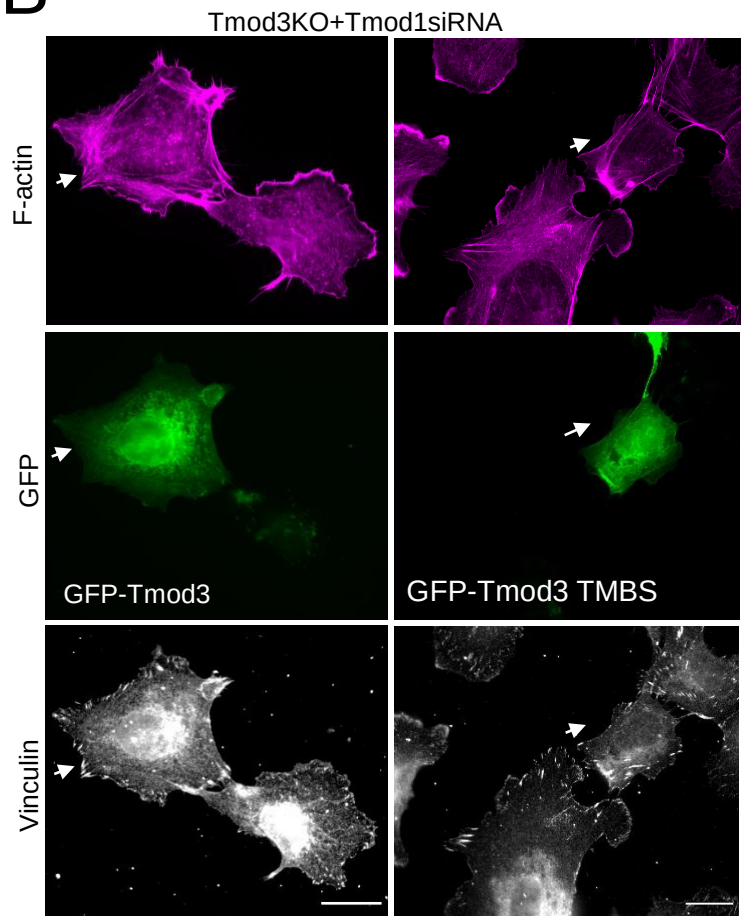

C

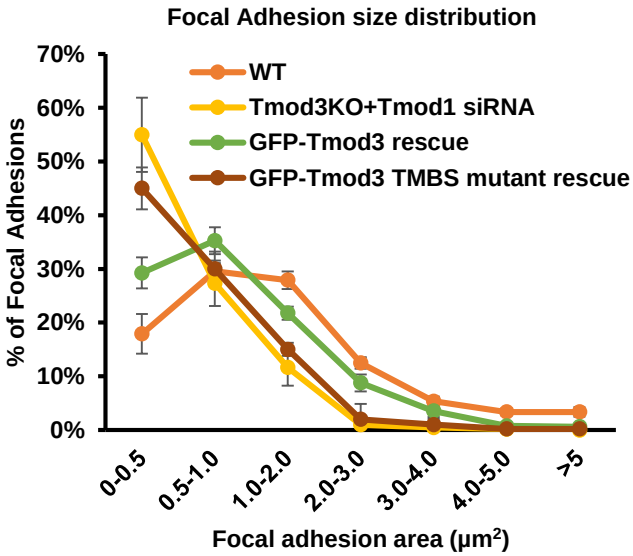

D

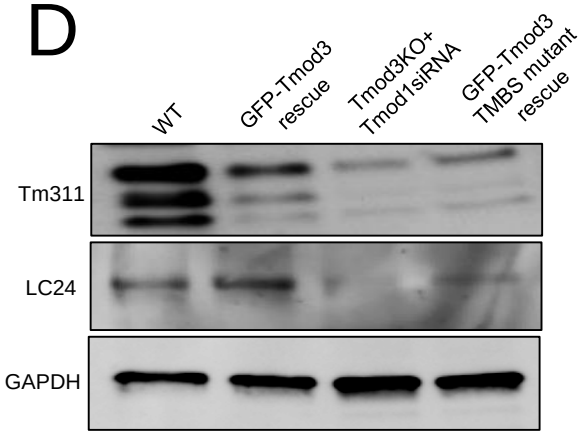

Figure S6

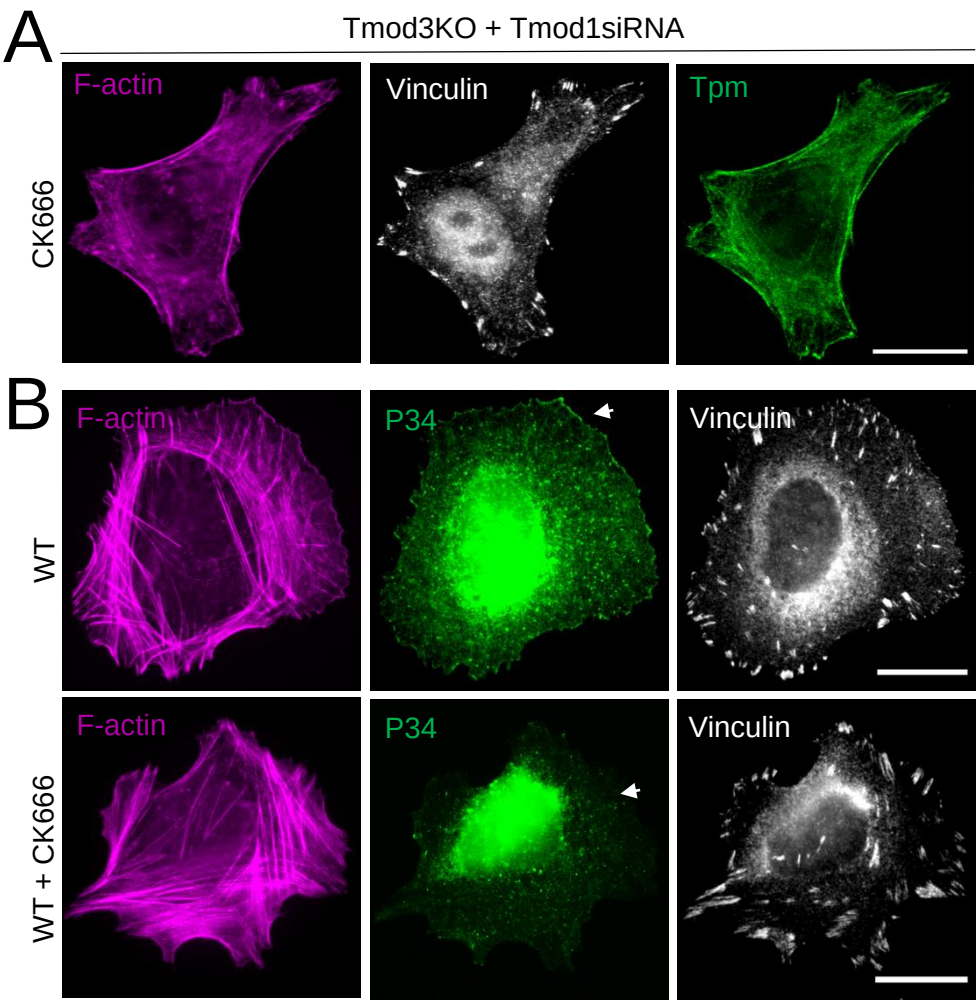
A
Tmod3KO + Tmod1siRNA
CK666
F-actin
Vinculin
Tpm
B
WT
WT + CK666
F-actin
P34
Vinculin

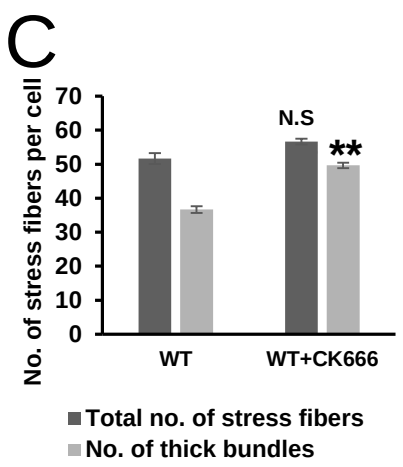
C
No. of stress fibers per cell
70
60
50
40
30
20
10
0
N.S
**
WT
WT+CK666
Total no. of stress fibers
No. of thick bundles

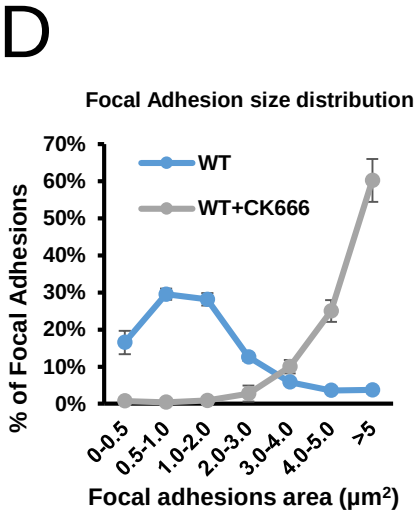
D
Focal Adhesion size distribution
% of Focal Adhesions
70%
60%
50%
40%
30%
20%
10%
0%
WT
WT+CK666
0-0.5
0.5-1.0
1.0-2.0
2.0-3.0
3.0-4.0
4.0-5.0
>5
Focal adhesions area (μm²)

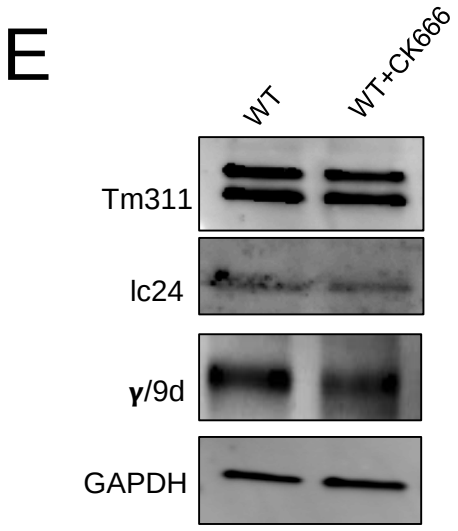
E
WT
WT+CK666
Tm311
lc24
γ/9d
GAPDH

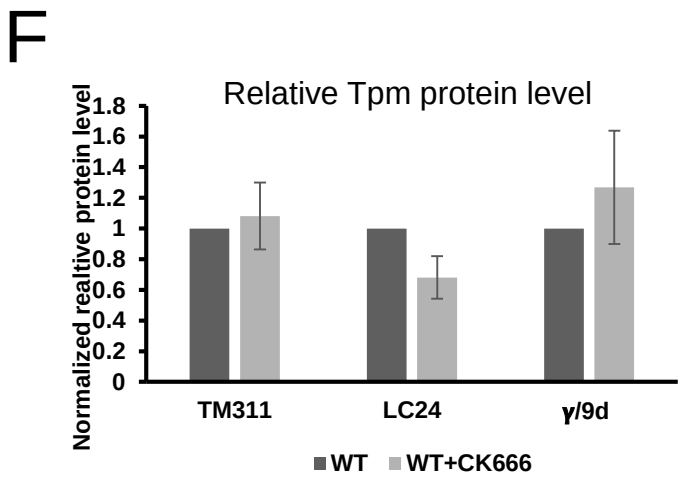
F
Relative Tpm protein level
Normalized realtive protein level
1.8
1.6
1.4
1.2
1
0.8
0.6
0.4
0.2
0
TM311
LC24
γ/9d
WT
WT+CK666

Table S1. Spectral count values of biotinylated proteins by BirA-tagged human TPM3 in U2OS cells. The data are from two independent experiments.

UniProt Accession	Protein Description	Sequence Coverage (%)	# Unique Peptides
P21333	Filamin-A OS=Homo sapiens OX=9606 GN=FLNA PE=1 SV=4 - [FLNA_HUMAN]	66.53	117
Strep-tag	Strep-tag	83.75	21
Q14315	Filamin-C OS=Homo sapiens OX=9606 GN=FLNC PE=1 SV=3 - [FLNC_HUMAN]	26.68	42
O75369	Filamin-B OS=Homo sapiens OX=9606 GN=FLNB PE=1 SV=2 - [FLNB_HUMAN]	26.86	41
P06753	Tropomyosin alpha-3 chain OS=Homo sapiens OX=9606 GN=TPM3 PE=1 SV=2 - [TPM3_HUMAN]	48.42	7
Q9Y490	Talin-1 OS=Homo sapiens OX=9606 GN=TLN1 PE=1 SV=3 - [TLN1_HUMAN]	13.81	25
P07355	Annexin A2 OS=Homo sapiens OX=9606 GN=ANXA2 PE=1 SV=2 - [ANXA2_HUMAN]	59.59	18
P09493	Tropomyosin alpha-1 chain OS=Homo sapiens OX=9606 GN=TPM1 PE=1 SV=2 - [TPM1_HUMAN]	33.8	2
P67936	Tropomyosin alpha-4 chain OS=Homo sapiens OX=9606 GN=TPM4 PE=1 SV=3 - [TPM4_HUMAN]	34.68	4
P07951	Tropomyosin beta chain OS=Homo sapiens OX=9606 GN=TPM2 PE=1 SV=1 - [TPM2_HUMAN]	26.41	1
Q9Y3F4	Serine-threonine kinase receptor-associated protein OS=Homo sapiens OX=9606 GN=STRAP PE=1 SV=1 - [STRAP_HUMAN]	42.29	11
Q9Y266	Nuclear migration protein nudC OS=Homo sapiens OX=9606 GN=NUDC PE=1 SV=1 - [NUDC_HUMAN]	27.79	10
P50479	PDZ and LIM domain protein 4 OS=Homo sapiens OX=9606 GN=PDLIM4 PE=1 SV=2 - [PDLI4_HUMAN]	41.21	10
Q9UHD8	Septin-9 OS=Homo sapiens OX=9606 GN=SEPT9 PE=1 SV=2 - [SEPT9_HUMAN]	18.09	6
Q16181	Septin-7 OS=Homo sapiens OX=9606 GN=SEPT7 PE=1 SV=2 - [SEPT7_HUMAN]	27.92	7
Q9NYL9	Tropomodulin-3 OS=Homo sapiens OX=9606 GN=TMOD3 PE=1 SV=1 - [TMOD3_HUMAN]	17.33	5
P49023	Paxillin OS=Homo sapiens OX=9606 GN=PXN PE=1 SV=3 - [PAXI_HUMAN]	13.54	5
O60664	Perilipin-3 OS=Homo sapiens OX=9606 GN=PLIN3 PE=1 SV=3 - [PLIN3_HUMAN]	18.43	5
Q9UPU7	TBC1 domain family member 2B OS=Homo sapiens OX=9606 GN=TBC1D2B PE=1 SV=2 - [TBD2B_HUMAN]	2.18	1
P0DP25	Calmodulin-3 OS=Homo sapiens OX=9606 GN=CALM3 PE=1 SV=1 - [CALM3_HUMAN]	29.53	3
Q8TCG1	Protein CIP2A OS=Homo sapiens OX=9606 GN=CIP2A PE=1 SV=2 - [CIP2A_HUMAN]	5.08	3
Q15417	Calponin-3 OS=Homo sapiens OX=9606 GN=CNN3 PE=1 SV=1 - [CNN3_HUMAN]	11.55	3
Q8N5W9	Refilin-B OS=Homo sapiens OX=9606 GN=RFLNB PE=1 SV=1 - [RFLB_HUMAN]	11.68	2
Q9UK76	Jupiter microtubule associated homolog 1 OS=Homo sapiens OX=9606 GN=JPT1 PE=1 SV=3 - [JUPI1_HUMAN]	25.97	2
Q14258	E3 ubiquitin/ISG15 ligase TRIM25 OS=Homo sapiens OX=9606 GN=TRIM25 PE=1 SV=2 - [TRI25_HUMAN]	5.71	3
Q5VU43	Myomegalin OS=Homo sapiens OX=9606 GN=PDE4DIP PE=1 SV=3 - [MYOME_HUMAN]	1.36	1